Renewable Energy 248 (2025) 123147

Contents lists available at ScienceDirect

Renewable Energy

journal homepage: www.elsevier.com/locate/renene

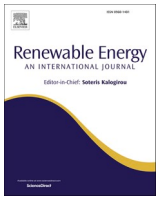

Medium-deep geothermal resources in the Molasse Basin: A geological, techno-economic, and ecological study of large-scale heat pump integration

Jaromir Jeßberger [a,*], Hannah Uhrmann [a], Felix Schölderle [b], Daniela Pfrang [b], Florian Heberle [a], Kai Zosseder [b], Dieter Brüggemann [a]

[a] Chair of Engineering Thermodynamics and Transport Processes (LTTT), Center of Energy Technology (ZET), University of Bayreuth, Prof.-Rüdiger-Bormann-Strasse 1, DE-95447, Bayreuth, Germany

[b] Chair of Hydrogeology, Technical University of Munich, Arcisstr. 21, DE-80333, Munich, Germany

A B S T R A C T

Medium-deep geothermal systems, with low exploration and investment costs, offer a solution to decarbonize the heating sector. The South German Molasse Basin (SGMB) is a reservoir with significant hydrothermal potential, where exploration has largely focused on depths greater than 2500 m. Here, medium-deep geothermal systems could provide water temperatures of 30 °C–80 °C. Large-scale heat pumps can raise supply temperatures for integration into district heating networks. While previous studies have concentrated on specific cases, this study adopts a more comprehensive approach, by examining the region of the underexplored northern SGMB. Geological parameters, such as depth, temperature, and water flow rates, were analysed to evaluate the techno-economic and ecological feasibility. At 1000 m depth, a base scenario with thermal water temperatures of 45.6 °C and a mass flow rate of 100 kg/s was evaluated. Following, sensitivity analyses varied geological parameters like depth and flow rate, based on the geological analyses, to represent the entire region, revealing *LCOH* between 77 and 151 €·MWh^{-1} and *GWP* between 53 and 136 kg CO_2 eq./MWh. These holistic analyses demonstrate the significant benefits of medium-deep geothermal systems combined with heat pumps for sustainable heating. And provide guidance to local authorities and operators.

1. Introduction

With a share of around 50 % of the European final energy consumption, the heating and cooling sector represents the dominating sector in terms of achieving the climate goals of the EU. Currently, only 24.8 % of the energy consumption in this sector are supplied by renewable energy sources [1], indicating a significant potential for decarbonization. Geothermal systems represent a renewable energy technology that can play an important role. However, the current focus is mainly on developing reservoirs with suitable temperatures for direct use in existing district heating Networks (DHN), i.e. geothermal temperatures above 80 °C, or enhanced geothermal systems with temperatures above 100 °C. In addition to this, medium-deep geothermal systems can also be integrated into the heat supply and further the expansion of renewable energies. This means that reservoir temperatures below 80 °C are used and coupled with large-scale heat pumps, to provide the required temperatures. This study focuses on the South German Molasse Basin (SGMB) as a potential hydrothermal heat source. The most promising horizons are the Lower Cretaceous and Upper Jurassic sediments that extend from the Alps up to the Franconian Alb with decreasing depth from the south and hence decreasing thermal water temperature. So far, utilization in the central part of the SGMB has concentrated on depth ranges from approx. 1500 m True Vertical Depth (TVD) and deeper. As of 2024, there are 18 geothermal heating plants in the greater Munich area that utilise geothermal energy from the Molasse Basin directly and provide heat or electricity [2]. An exemplary heating project at 80 °C and 1970 m drilling depth is Unterschließheim (Dussel et al. [3]). Almost all projects are related to a production temperature of the geothermal fluid between 80 °C and 140 °C [2]. Increasing demand for low carbon energy sources and advancing technological progress are driving the further development of geothermal energy. The expected production temperature conditions in the northern part of the SGMB vary between 30 °C and 80 °C. First estimations underline the large growth potential of medium-deep geothermal resources in this region (see Weber et al. [4]). In this context, the term "medium-deep geothermal energy" is defined as follows in this study: the reservoir depth is less than or equal to 2500 m or and the temperature is less than or equal to 80 °C. These kinds of systems allow the use of a drilling technique for shallower depths. The heat can only be utilized directly in 4th generation DHN on a low temperature level, otherwise the

* Corresponding author. Chair of Engineering Thermodynamics and Transport Processes (LTTT), Center of Energy Technology (ZET), University of Bayreuth, Prof.-Rüdiger-Bormann-Strasse 1, DE-95447, Bayreuth, Germany.

E-mail address: jaromir.jessberger@uni-bayreuth.de (J. Jeßberger).

https://doi.org/10.1016/j.renene.2025.123147

Received 17 December 2024; Received in revised form 20 March 2025; Accepted 11 April 2025

Available online 12 April 2025

downstream connection of a heat pump is required. In literature, such systems are also called low-energy geothermal production plants. In Paris and the Aquitaine Basins, 65 of these medium-deep systems based on hydrothermal reservoirs are in operation in 2005 (Laplaige et al. [5]). In addition, most of the scientific literature contains case studies on medium-deep geothermal systems based on coaxial heat exchangers. Corresponding studies examine selected heat transfer fluid or the surrounding solid material for selected cases or boundary conditions [3,5,6]. While the research to date has improved the understanding of medium-depth geothermal systems, an important research gap remains: Most existing studies are limited to isolated case studies, which limits the scalability and broader applicability of the results. There is a lack of comprehensive regional-level analyses that assess the potential of medium-deep geothermal energy in combination with large heat pumps to supply DHNs. This kind of holistic analysis is conducted for deep geothermal systems under consideration of geological potential and techno-economic aspects of geothermal power plants for electricity generation [4,7]. This study closes research gaps for medium-deep geothermal systems by analysing hydrothermal reservoirs on a regional level and evaluating the technical, economic and environmental feasibility of integrating large-scale heat pumps into existing district heating networks with a temperature of 100 °C based on geological models.

The paper is divided in three parts whereas each part contains a detailed literature review elaborating the specific research gap to be closed (see Chapters 2.1, 3.1 and 4.1), methodology and the presentation and discussion of the results. First, the boundary conditions from a geological perspective are determined by presenting the available database and defining a method to predict the geothermal water temperature and extraction flow rate based on the drilling depth required to reach the reservoir. For hydrothermal utilization of the SGMB, it is common practice to drill through the entire thickness of the reservoir. The drilled reservoir section is therefore added to the depth to top reservoir, which is assumed to be an expected uniform reservoir thickness for the medium-deep region of the SGMB. Then, a comprehensive techno-economic analysis is conducted based on the defined geological boundary conditions to evaluate the potential of integrating large-scale heat pumps to provide renewable heat for existing DHN. In this configuration, the supply temperature of the DHN is provided by the large-scale heat pump. Especially, the large-scale heat pumps at MW scale are underrepresented in the literature (see Chapter 3.1). In order to structure this approach, a base scenario is defined and analysed within a techno-economic framework. Subsequently, the analysis is expanded through sensitivity analyses, in which essential technical and economic parameters are varied, including exploration costs, surface technology requirements, and geological boundary conditions, occurring in the analysed region. In particular, the levelized costs of heat (*LCOH*) are calculated based on these factors, forming the foundation of the economic assessment. To comprehensively address the environmental impacts, a detailed life-cycle assessment (LCA) is conducted. The LCA evaluates relevant impact categories for the geothermal sector with a special focus on greenhouse gas emissions based on input and output inventories, thereby providing a more accurate representation of real-world market-based emissions. In contrast to the typical approach to renewable heat, which frequently assumes a fully renewable electricity mix, this assessment considers the changing electricity mix over the lifetime, making it particularly relevant in light of the European Union's Technical Expert Group on Sustainable Finance's threshold of 100 g CO_2/kWh for energy generation. This threshold will decrease every five years until it reaches net zero by 2050 [8]. It is therefore imperative to accurately define the system's environmental impact in order to align with the aforementioned climate targets which are especially of interest for the operators.

Concluding, the novelty of this study is highlighted in several areas. First, hydrothermal reservoirs are analysed, distinguishing this study from most prior work on medium-deep systems, (comparative case studies and assessments of closed borehole heat exchangers and deep geothermal systems are mentioned, e.g. Zhu et al. [9]). Furthermore, a regional-scale analysis with a holistic and interdisciplinary approach is conducted here, allowing for scalability and broader applicability (see Chapter 2; for examples of regional analyses, see Wang et al. [10]). Additionally, a focus is placed on centralized heat pump systems on a megawatt scale, diverging from the decentralized configurations commonly examined in existing studies (see Chapter 3.1). Following an initial discussion of geological boundary conditions, the system is assessed from both techno-economic and ecological perspectives. This is of particular interest due to regulatory aspects. In 2024, the Heating Planning Act came into force in Germany, requiring the federal states to prescribe municipal heat planning for individual communities. In January 2025, when it came into force in Bavaria [11], geothermal energy came more prominent as a renewable source of heat in regions with high potential. In this context, developed and well-studied reservoirs are of equal interest as alternative, undeveloped reservoirs. This indicates that the demand from municipal customers will continue to increase, and therefore the consideration of an entire region in this study is very beneficial for decision-makers.

2. Geology

This chapter discusses the hydrogeophysical parameters of the Lower Cretaceous and Upper Jurassic sediments regarding utilization as a hydrogeothermal reservoir in the central part of the SGMB in Bavaria.

2.1. Fundamentals

In geothermal systems in which the heat is extracted from natural aquifers, typically a hydrogeothermal doublet (Fig. 1) consisting of a deviated production and injection well is implemented. Via electrical submersible pumps (ESP), the warm water is transported to the surface where it is directly used or transferred to a heat exchanger in a second cycle (Stober and Bucher [12], DiPippo [13]). After heat extraction, the cooled water is re-injected in the second well at a decent distance to the production well to avoid thermal interference. To operate the hydrogeothermal system most successfully and efficiently, the highest possible thermal output is required, which is mainly determined by the flow rate and production temperature of the fluid (Stober and Bucher [12], Zosseder et al. [14]).

The Lower Cretaceous ('Purbeck') and Upper Jurassic ('Malm') reservoir is already widely used in the SGMB to generate geothermal energy. These two geological units form an extensive water reservoir

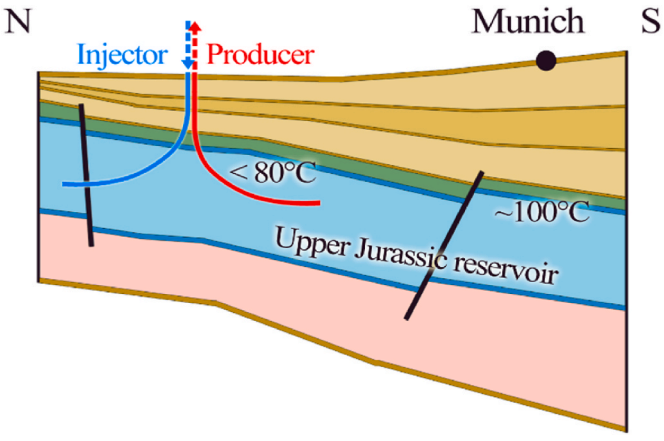

Fig. 1. Sketch of a geothermal doublet tapping into the yet undeveloped shallower Upper Jurassic reservoir in the northern part of the South German Molasse Basin, where production temperatures of well below 80 °C are expected.

that dips from the Franconian Alb in the north to the northern border of the Alps. Hydrostratigraphically, the carbonate sediments of the Lower Cretaceous and the Upper Jurassic are in contact and form the reservoir referred to here simply as the Upper Jurassic [15]. These sediments can reach thicknesses of up to 600 m [16] and consist of alternating shallow marine sequences of limestones, marls and dolostones [17].

In general, the geological requirements for a productivity forecast are the depth of the top reservoir and the thickness of the reservoir, as these directly affect the drilling costs. In addition, the production temperature $T_{source,in}$, possible injection temperature T_I and brine mass flow rate $\dot{m}$ define the possible thermal power P_{th} (eq. (1), Stober and Bucher [12]):

$$P_{th} = c_p \cdot \dot{m} \cdot \left(T_{source,in} - T_I\right) \quad (1)$$

With c_p being the specific heat capacity of the thermal fluid.

2.2. Methodology and data base

Since the scope of this study is the shallower region in the SGMB, which has a lower production temperature than 80 °C and has not yet been developed by geothermal wells, underground information is largely missing. Accordingly, many assumptions must be made, and the uncertainties are therefore high. Fig. 2 shows the geothermal wells already in operation in the southern part of the study area where the temperature is higher, and the reservoir is deeper as well as the cooler regions in the north that are not developed so far. From borehole data, literature and free available geological data, we define the key reservoir related parameters: depth of top reservoir, reservoir thickness, production temperature, and production rate.

2.2.1. Top reservoir and reservoir thickness

The depth of the top reservoir is taken from the free available geothermal information system GeotIS [20] and the thickness of the Upper Jurassic sediments from Bachmann et al. [18] and Böhm [16]. As shown in Fig. 2, the reservoir can be expected to be at least 400 m thick for a large part of the basin north of the 80 °C boundary shown, where cooler production temperatures are expected.

2.2.2. Production temperature

The production temperature can be specified as a function of the depth of top reservoir from an available temperature map. GeotIS also provides a depth temperature (undisturbed temperatures on top of the reservoir; [20,21]), but in general, in conductive dominated reservoir systems, such as the SGMB, the production temperature is a function of the depth of flow zones. However, the geothermal gradients within the SGMB vary considerably, so that regional thermal anomalies occur. For example, there is a positive anomaly (higher temperatures than average) in the Munich area and a significant negative anomaly east of Munich in the so-called 'Wasserburg Through' [20–22].

To take a conservative approach, the GeotIS temperatures at Top Malm were taken as the expected production temperatures. ArcGIS Pro [23] was used to calculate distributions for the reservoir depth with production temperature thresholds in steps of 10 from 30 °C to 80 °C with the statistical analysis tools of ArcGIS Pro. The 10 percentile (P10), 90 percentile (P90) and modal value for each temperature value were entered as inputs for the techno-economic analysis, described in the

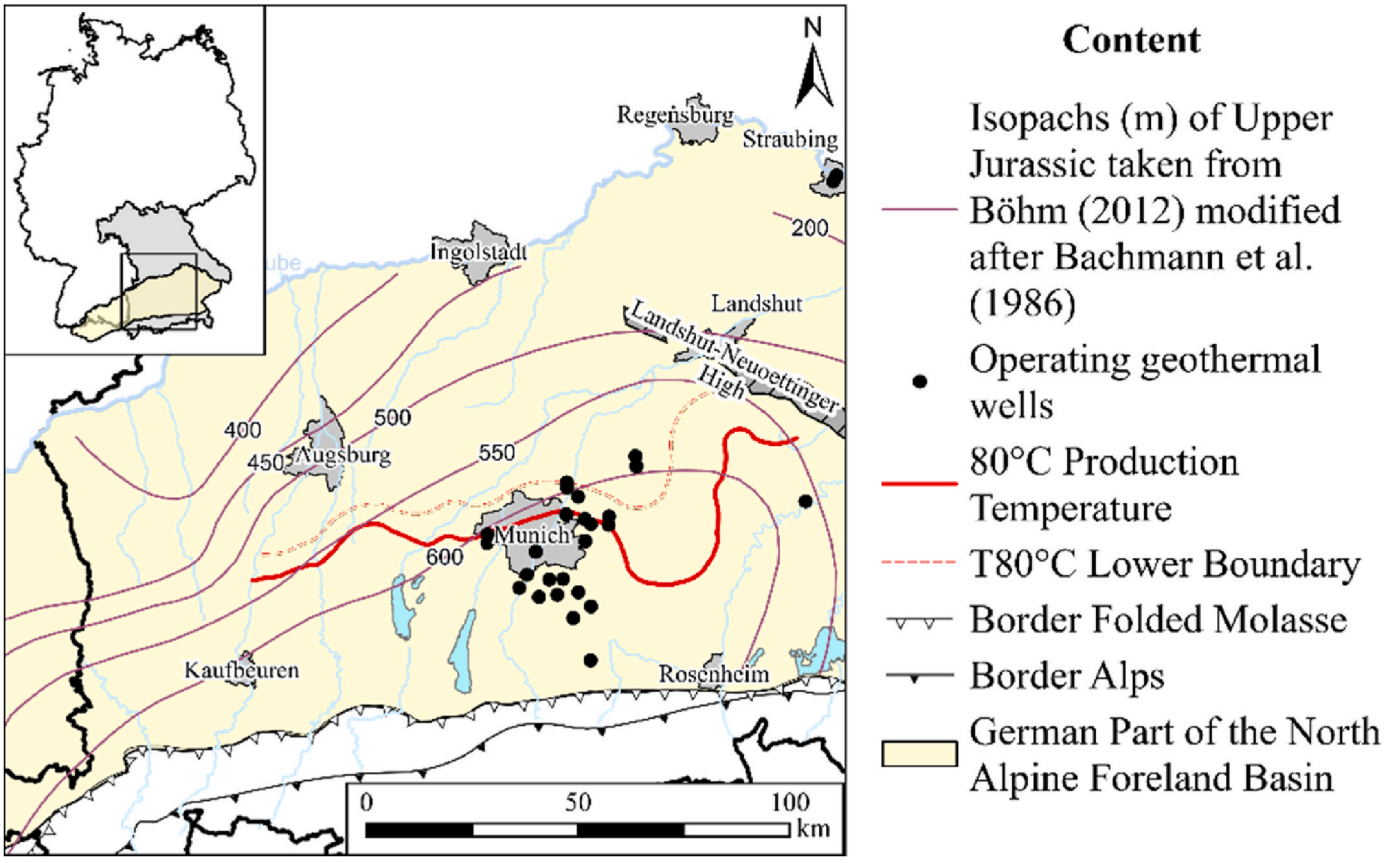

Fig. 2. North Alpine Foreland Basin in SE Germany with operating geothermal wells, isopaches for the Upper Jurassic reservoir after Bachmann et al. [18] and Böhm [16], and the border south of which production temperatures of over 80 °C are likely to be suitable for direct injection into a district heating network. The 80 °C border was calculated by regressing the GeotIS temperatures with known outflow temperatures in the area and the light red dashed line represents the uncertainty range of this regression. (see Keim et al. [19], Zosseder et al. [14]). (For interpretation of the references to colour in this figure legend, the reader is referred to the Web version of this article.)

following chapter, as shown in Table 1. The regionally varying geothermal gradients in the SGMB are reflected in Table 1 in the different ranges of P10 and P90 values. As can be seen in Table 1, some of the values are distributed skewed, particularly noticeable at the 50 °C, 70 °C and 80 °C isotherm. This is due to regionally limited thermal anomalies, such as the 'Wasserburg Through' east of Munich (see Fig. 2), where temperatures of 70 °C and 80 °C are expected at much higher depths than in the rest of the basin. This leads to a skewed distribution with a modal value shifted towards the P10 value.

2.2.3. Production rate

There is a lack of empirical values for the reachable mass flow rate for the area in question. Therefore, values known from the geothermal boreholes in the southern part of the area must be considered. Since the northernmost geothermal wells in the study area (near the 80 °C limit) have high porosity and permeability, the shallower parts of the reservoir are also believed to have good hydraulic properties with mean porosity of the Upper Jurassic 'Zeta' interval of >10 %. [14]. A rough estimate of 30 kg/s – 200 kg/s mass flow rate is therefore considered. A further classification or correlation is not possible here.

3. Integration of large-scale heat pumps into medium-deep systems

This chapter discusses the technical and economic aspects of integrating large-scale heat pumps in the geological region presented previously.

3.1. Fundamentals

The integration of large-scale heat pumps into geothermal energy systems has been investigated in different studies. A corresponding literature review is given, to elaborate the research gap in the context of an integration in DHN. The heat pump market is experiencing significant growth. Arpagaus et al. [24] identified 26 commercially available large-scale high-temperature heat pumps (HTHPs) with maximum supply temperatures exceeding 90 °C, with investment costs ranging from 100 €/kW to 1000 €/kW [25]. Market-ready technologies offer heating capacities from 20 kW to 20 MW. Jiang et al. [26] conducted a review of the current state of HTHPs, highlighting four promising areas: low-*GWP* refrigerants, supply temperatures above 100 °C, heating capacities exceeding 1 MW, and *COP*s greater than 4 at a temperature lift of 40 K. Adamson et al. [27] identified in their literature review a huge potential of transcritical cycles to reach supply temperatures above 200 °C with suitable system efficiencies. Khalid et al. [28] evaluated the potential of HTHP integration into industrial processes, by examining different integration concepts, research and development opportunities as well as barriers of the technology. Finally, Barco-Burgos et al. [29] analysed several integration concepts of HTHPs into district heating and cooling networks. The different generations of DHNs were studied and twelve integration concepts technically evaluated. Apart from the review publications, there are a lot of research articles dealing with the integration of large scale and high-temperature heat pumps into different sink systems. Kosmadakis et al. [30] investigated the integration into industrial processes and, thereby, the upgrade of waste heat up to 150 °C. The authors also examined different plant configurations like a simple HTHP cycle, the use of an internal heat exchanger and two-stage compression. Dumont et al. [31] examined the integration of HTHPs in the food and beverages industry. Their results indicated that HTHPs could meet 12 TWh/a of process heat demand in the German food and beverages industry. The combination of geothermal energy systems and HTHPs or large-scale heat pumps was investigated in different aspects. Mateu-Royo et al. [32] investigated the integration of HTHPs into DHNs. The DHN serves as both a heat sink and a heat source in their operations. It acts as a heat sink when waste heat from a supermarket refrigeration system is utilized, and as a heat source when industrial customers have heating needs. Arslan et al. [33] evaluated the combination of existing DHN with thermal energy storages and heat pumps. They conducted a multi-objective parameter optimization to obtain a high performing combination of different variables like refrigerant and phase change material. Liu et al. [34] conducted a thermal analysis of a DHN coupled with a deep open looped geothermal well and a heat pump, with focusing on the economic optimization of the system. Sartor et al. [35] investigated the integration into a DHN with a focus on steam production and the behaviour of the *COP* of the HTHP. Dimitriu et al. [36] evaluated the combined utilization of geothermal water and contained gas by using heat pumps and gas turbines. The heat pump is able to cover over 70 % of the peak load of a DHN in winter by using the reinjection mass flow as heat source. The combination of geothermal heat source and large scale heat pumps was also examined by Jensen et al. [37], to identify the most suitable system configuration of two heat pumps connected in series. Jeβberger et al. [38] showed the potential of the integration of large scale heat pumps into existing geothermal energy systems and conducted different sensitivity analyses with a techno-economic point of view. Deng et al. [39] investigated the combination of medium-deep geothermal boreholes with heat pumps focusing on optimizing the system for supply temperatures up to 55 °C. Arslan et al. [40] analysed with an exergoeconomic point of view the upgrade of a medium-deep geothermal system. They analysed the influence of different refrigerants on the net present value and identified an optimum solution for the presented case study.

The presented review shows the relevance of integrating large scale heat pumps into industrial processes as well as for the planning of municipal heating systems. The case studies mostly address specific use cases with fixed boundary conditions and corresponding heat pump scales, for deep geothermal applications or industrial waste heat utilization. So, the research gap addressed in this study, is to give an overview of the techno-economic aspects of the integration of large-scale heat pumps into medium-deep geothermal energy systems, with varying the geological boundary conditions, referred to the previous presented geological analysis for the SGMB.

3.2. Methodology

In this chapter, the methodology and the boundary conditions for the techno-economic analyses are presented. The examined system consisting of the geothermal heat source, the heat pump and the DHN is visualized in Fig. 3.

Exemplarily, the geothermal heat source at a depth of 1000 m, offers a supply temperature of 45.6 °C at the top of the reservoir, defines the base scenario of this study. See Equation (2) based on modal values in Table 1.

$$T_{source,in} = 41.925 \cdot \ln(depth) - 243.97 \quad (2)$$

The drilling depth then corresponds to the depth of the top of the reservoir and additionally the thickness of the reservoir (which can be estimated to 400 m, see Fig. 2). The reinjection temperature is limited to a minimal value of 20 °C and the difference between thermal water temperature and the reinjection temperature is kept constant at 20 K, when the reinjection temperature limit is met. The district heating

Table 1
Production temperatures as a function of the depth of top reservoir.

Production Temperature at Top Reservoir (°C)	Depth Top Reservoir (m)		
	P10	P90	Modal Value
30	500	800	**650**
40	700	1000	**900**
50	900	1250	**1250**
60	1050	1800	**1450**
70	1300	3000	**1600**
80	2100	3800	**2250**

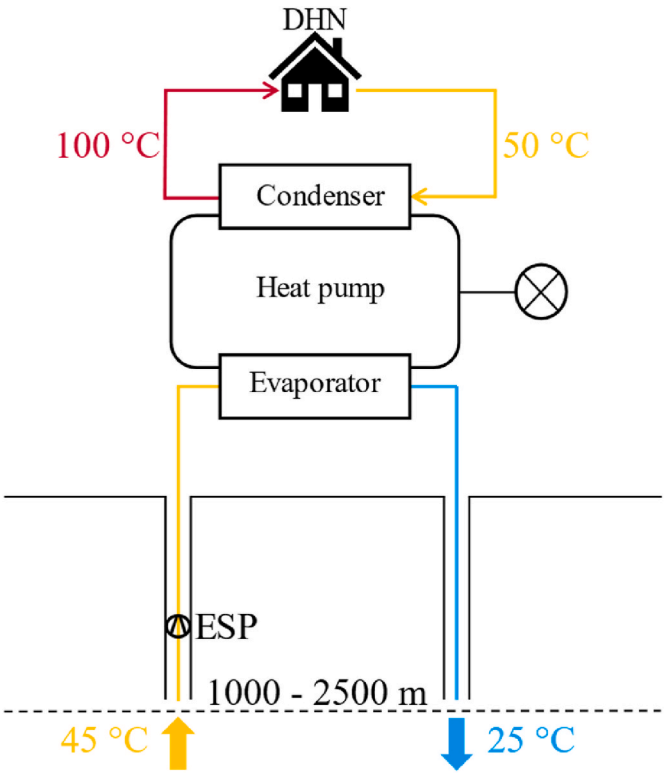

Fig. 3. Medium-deep geothermal district heating network with a large-scale heat pump, with temperatures of the base scenario.

network on the heat sink side is operating with a supply temperature of 100 °C, which corresponds to an existing DHN of 3rd generation (compare Mazhar et al. [41]). The return temperature is set to 50 °C. To pump the water to the surface and into the heat exchangers, electric submersible pumps (ESPs) are commonly used. The technology is transferred from the oil and natural gas industry, which leads to several challenges caused by corrosive properties and increased gas content in the thermal water. As stated by Jeßberger et al. [42] there is a huge potential to decrease the levelized cost of heat (*LCOH*) by optimizing the performance and replacement procurements of the ESP. The calculation of the electrical energy consumption of the ESP is crucial for techno-economic analysis. Therefore, boundary conditions according to Table 2 are defined and the calculations are carried out for every analysed case. The pressures are adapted from an exemplary deep well project in the study area.

As shown in Fig. 4, the ESP is located below the geothermal water level, taking the maximum water drop caused by reservoir fluctuations into account. Due to location-dependent differences in the maximum water drop, the installation depth H_{geo} is set to 15 % of the drilling depth (including the additional 400 m drilling in the reservoir).

Additionally, Fig. 4 illustrates a scheme of well completion as can be assumed for the shallower part of the study area. On the right-hand side (b of Fig. 4), the reinjection well, and on the left-hand side (a of Fig. 4) the production well are drawn with the bitsize (BS), outer diameter (OD)

Table 2
Boundary conditions for the design of the ESP.

Installation depth; H_{geo}	0.15 · drilling depth
Standpipe diameter; d	0.2244 m
Pressure at pump inlet; p_{in}	2 MPa
Pressure at pump outlet; p_{out}	1.5 MPa
Tube roughness; ε	0.25 mm
Density; ρ	987 kg/m^3
Volume flow; $\dot{V}$	Use case depending
Pump efficiency; η_{elec}	0.7

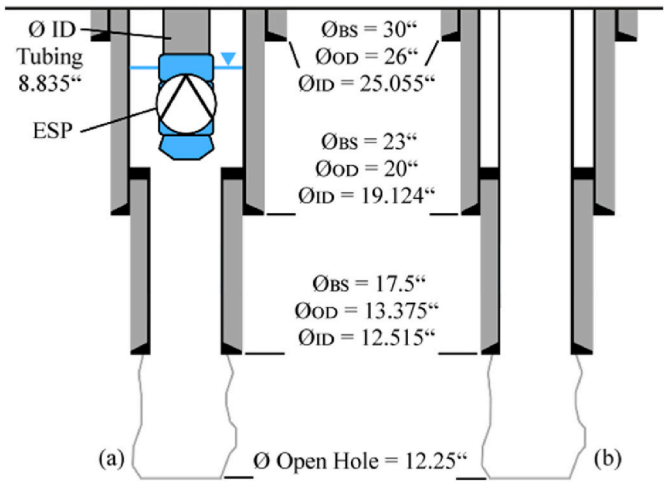

Fig. 4. Scheme of the production well (a) and reinjection well (b).

and inner diameter (ID). This completion is assumed as the standard case for this study for a first approach. For the estimation of the required power consumption of the ESP, the flow regime of the geothermal water has to be evaluated first, by calculating the Reynolds number:

$$Re = \frac{w \cdot L \cdot \rho}{\eta} \tag{3}$$

Where L is the characteristic length and corresponds to the inner diameter d esp. ID, w the flow velocity, ρ the density and η the dynamic viscosity. For Reynolds numbers

$$Re > 2320, \tag{4}$$

the flow is turbulent. However, between $Re = 2320$ and $Re = 8000$ and in case of hydraulically smooth tubes, the flow can be laminar. Therefore, it is necessary to evaluate whether the flow occurs within the regime of hydraulically smooth or rough tubes based on the tube roughness ε (see Table 2). According to Moody [43] the flow is characterized as hydraulically rough tubes, in case of

$$Re \cdot \frac{\varepsilon}{d} > 1300. \tag{5}$$

For a hydraulically rough tube the tube friction coefficient λ depends only on the tube roughness and on the geometry:

$$\lambda = \frac{1}{\left(2 \cdot log\left(3.71 \cdot \frac{d}{\varepsilon}\right)\right)^2} \tag{6}$$

In the transition zone the Moody chart is used to determine the tube friction coefficient [43]. With λ, the pressure losses Δp_v can be calculated using Equation (7):

$$\Delta p_v = \lambda \cdot \frac{L}{d} \cdot \frac{\rho}{2} \cdot w^2 \tag{7}$$

where L is the length of the tube (H_{geo}). With the pressure losses, the installation depth (H_{geo}), the radius r, and the pressure difference between pump inlet and the heating station the required discharge head H_A can be calculated:

$$H_A = H_{geo} + \frac{(p_{out} - p_{in})}{r \cdot g} + \frac{(w_{out}^2 - w_{in}^2)}{2 \cdot g} + \frac{\Delta p_v}{r \cdot g} \tag{8}$$

Where p_{out} is the pressure at the heating station, p_{in} the pressure at the pump inlet and r the radius. The velocity is assumed as constant. This leads finally to the ESP electrical power:

$$P_{\text{Pump}} = H_A \cdot \rho \cdot g \cdot \dot{V} \cdot \eta_{\text{elec}} \tag{9}$$

Referring to Schlagermann [44] the capital-related costs of the ESP system depend on the installed hydraulic power and can be calculated with

$$c_{\text{power specific}} = P_{\text{Pump}} \cdot \left(11,685 \cdot P_{\text{Pump}}^{-0.319}\right) \tag{10}$$

and quantity specific costs including the standpipe, cables, installation and removal as well as personnel costs:

$$c_{\text{quantity specific}} = 5000 \cdot \left(\frac{H_{\text{geo}}}{250} + 4\right) + 10,000 \tag{11}$$

Both costs shares are summed up:

$$c_{\text{ESP}} = c_{\text{power specific}} + c_{\text{quantity specific}} \tag{12}$$

Including an additional cost of 10 % of the ESP investment costs in the base scenario lead to 706 k€. Next to the ESP, the heat pump system has to be technically and economically described. The efficiency of a heat pump is defined by the *COP*:

$$COP = \frac{\dot{Q}_{\text{heat sink}}}{P_{elec}} \tag{13}$$

With the thermal capacity of the heat pump $\dot{Q}_{\text{heat sink}}$ and its electrical power consumption P_{elec}. The thermodynamic maximum possible *COP* is defined by the Carnot efficiency:

$$COP_{\text{Carnot}} = \frac{T_{\text{sink,out}}}{T_{\text{sink,out}} - T_{\text{source,in}}} \tag{14}$$

Where $T_{\text{sink, out}}$ is the outlet temperature of the heat sink, in this case the supply temperature of the DHN. $T_{\text{source, in}}$ is the inlet temperature of the heat source, in this case the thermal water temperature. In this study, in order to facilitate the execution of a large number of sensitivity analyses, the heat pump model is simplified and a *COP* of 45 % of the Carnot-*COP* is assumed. The average Carnot-*COP* of industrially available HTHPs is between 40 % and 60 % (compare Jeβberger et al. [45], Arpagaus et al. [46], Jiang et al. [47], and Agora Energiewende [48]), so this assumption is a conservative boundary condition that will be varied in the following sensitivity analyses. Fig. 5 (published by Jeβberger et al. [45]) shows the *COP* of commercially available HTHPs and scientific test rigs as function of the temperature lift with Carnot efficiencies between 30 % and 60 %, except for a few outliers. The Carnot-*COP* of 45 % leads to a *COP* of 3.09 in the base scenario presented.

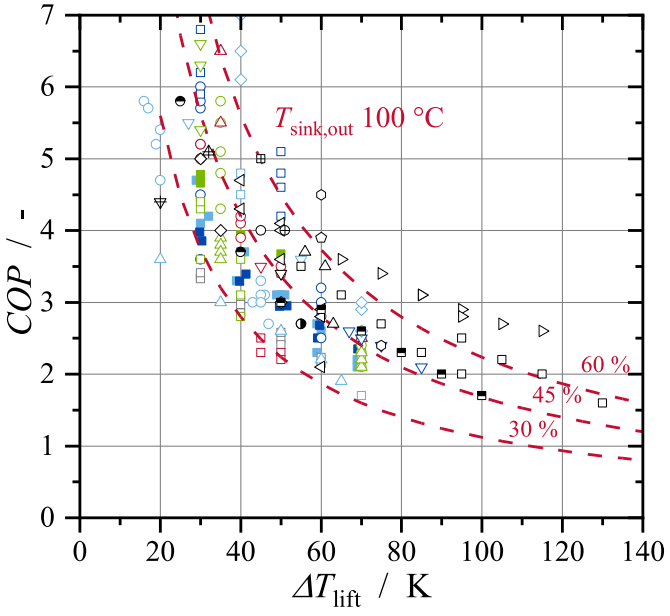

Fig. 5. *COP* as function of the temperature lift for different commercial HTHPs (black and white) and laboratory test rigs (coloured), with the trend line for Carnot efficiencies (taken from Jeβberger et al. [45]).

The heat demand of the DHN as function of time underlying this investigation is presented in a normalised diagram in Fig. 6. The figure shows, that the thermal capacity is reduced down to 10 % of the maximum load at summer days, which has to be considered in the planning process of DHNs and the corresponding over surface systems.

Based on the characterization of the ESP and the heat pump, the *LCOH* are calculated using the annuity method, regarding VDI guideline 2067 [49]. This method is a dynamic investment calculation using the annuity factor *a* presented in Equation (15) to make a forecast for the annual costs during the observation period *t*.

$$a = \frac{q^t \cdot (q-1)}{q^t - 1} \tag{15}$$

Where *q* is the interest rate. The costs are divided into different categories, the capital-related costs, the operation-related costs (e.g. service and maintenance), demand-related costs, which are dominated by the electricity demand, the miscellaneous costs which are neglected in the following and the proceeds. The annuity of the capital-related costs ($A_{\text{N,K}}$) can be calculated with Equation (16), where A_0 are the initial investment costs.

$$A_{\text{N,K}} = A_0 \cdot a \tag{16}$$

For the operation-related and the demand-related costs the price dynamic value factor b_x is introduced:

$$b_x = \frac{1 - \left(\frac{r_x}{q}\right)^t}{q - r_x} \tag{17}$$

where r_x is the annual increase of the concerning costs, based on the average inflation of the last 30 years [50]. Consequently, the annuity of the demand-related costs ($A_{\text{N,V}}$) and the operation-related costs ($A_{\text{N,B}}$) are calculated as in the following:

$$A_{\text{N,V}} = A_{V1} \cdot a \cdot b_V \tag{18}$$

$$A_{\text{N,B}} = A_{\text{B1}} \cdot a \cdot b_b + A_{\text{IN}} \tag{19}$$

with

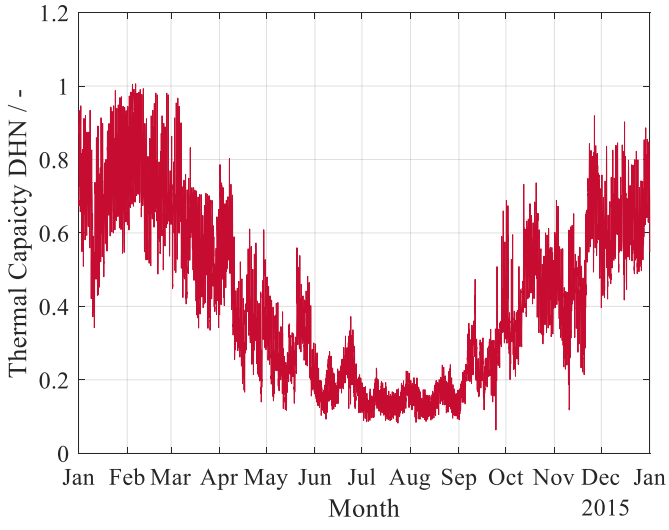

Fig. 6. Normalised annual heat demand of a district heating network.

$$A_{IN} = A_0 \cdot \left(f_{m+insp} + f_{inst}\right) \tag{20}$$

Where $f_{m\,+\,insp}$ is the factor for the expense for servicing and inspection and f_{inst} the factor for repairs [49]. Finally, the proceeds can be calculated with Equation (21).

$$A_{NE} = E_1 \cdot b_E \tag{21}$$

Where E_1 is the proceed in the first year and b_E is the price-dynamic cash value factor for the proceeds. Following, the annuity of the annual costs can be calculated:

$$A_N = A_{NE} - \left(A_{N,K} + A_{N,V} + A_{N,B}\right) \tag{22}$$

With an interest rate q of 1.05 [51] oriented on the policy rate of the European Central Bank, and an additional safety margin for a conservative calculation and an observation time t of 20 years, the annuity factor is 0.8. Additionally, the input parameters in Table 3 presented are considered.

With the thermal energy provided per year (Q_{sink}) and a neglection of the proceeds, the *LCOH* lead to:

$$LCOH = \frac{A_N}{Q_{sink}} \tag{23}$$

After the evaluation of the presented base scenario, different sensitivity analyses are carried out, to investigate the influence of different parameter variations on the *LCOH*. Another important performance parameter for the economic evaluation is the payback period (*PBP*). Using the capital value method, regarding VDI guideline 6025 [56], the capital value leads to:

$$K = -A_0 + \sum_{t=1}^{n} \frac{E_t - A_t}{q^t} \tag{24}$$

With the capital value K, the proceeds in the first year E_t and the demand-related costs in the first year A_t. Setting the capital value to zero and converting the equation to t, the *PBP* can be calculated.

3.3. Results

In this chapter, the results of the techno-economic analyses are presented with focus on the modal values for the model of geothermal reservoir (see Table 1). With 8.2 % for the ESP operation and 91.8 % for the heat pump operation, the analysis of the base scenario with respect to the annuity method shows the dominating impact of the demand related costs (see Fig. 7).

The operation-related costs for the geothermal system are neglected because the replacement procurements of the ESP already include the personnel costs, as stated previously. So, the operational costs are related to the cleaning of the heat exchangers, what is also included in the maintenance of the heat pump. The capital related costs show a very balanced result, with 46.6 % for the geothermal system. This share will increase drastically by increasing the required drilling depth. Table 4 shows the most important results of the techno-economic analysis.

Table 3
Boundary conditions for the economic analyses.

Observation period; t_{ob}	30 a
Interest rate; q	1.05 [51]
Price increase factor; r_x	1.02 [50]
Drilling costs; $c_{drilling}$	2000 €·m^{-1} [52]
Investment costs HTHP; c_{HTHP}	500 €·kW^{-1} [53]
Investment costs ESP; c_{ESP}	Equation (12)
Service life HTHP	20 a [49]
Service life ESP	7 a [54]
Service factor; $f_{m\,+\,insp}$	1 % [49]
Repair factor; f_{inst}	1.5 % [49]
Electricity price; c_{elec}	192.50 €·MWh^{-1} [55]
Thermal losses	3 % [38]
Electrical losses	7 % [38]
Full load hours; t_{fl}	4000 h·a^{-1}

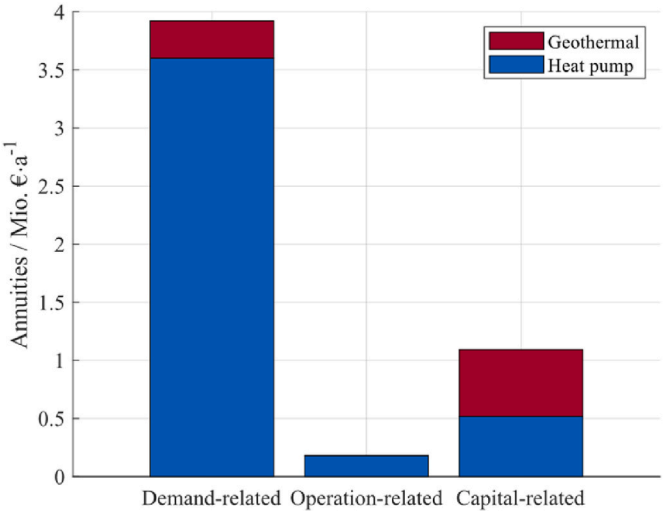

Fig. 7. Cost shares of the base scenario.

The *COP* leads with a temperature lift of 54.36 K and a supply temperature of 100 °C to 3.09. Taking the electrical power consumption of the ESP into account, the *COP* of the entire geothermal system is 2.84. With a mass flow rate of 100 kg s^{-1} of the brine, the maximum thermal capacity is 11.5 MW. Taking the full load hours of 4000 per year and the overall annuity into account, the *LCOH* in the base scenario lead to 113 €·MWh^{-1}. This puts the *LCOH* in a similar range to that calculated by Agora Energiewende [48] for large-scale heat pumps combined with geothermal systems. A detailed validation with other studies is difficult to carry out, in fact of the strong influence of the boundary conditions like reservoir characteristics, influencing the drilling costs, the electricity price which is highly depending on the location and required temperature lifts. Here, subsidies are not considered due to large variation in regulatory frameworks. For a medium customer selling price in Germany of 147 €·MWh^{-1} [57], the proceeds would lead to 34 €·MWh^{-1} and the *PBP* is 5 years. The accuracy of every economic analysis depends on the chosen boundary conditions, so in the following, sensitivity analyses are carried out, to see the influence of different parameters as well as of the location of the *DHN* in the SGMB.

3.4. Sensitivity analyses

The geological parameters can drastically influence the economic viability of the project. So, in Fig. 8 the drilling depth and the mass flow rate of the brine are varied to evaluate the influence of changing geological boundary conditions on the economics. The drilling depth varies as stated in chapter 0 from 1000 m to 2500 m. With changing the required drilling depth, depending on the location in the SGMB, the thermal water temperature is varied referred to Equation (2)

Table 4
Base scenario results of the techno-economic analysis.

COP [−]	3.09
System-*COP* [−]	2.84
$T_{source,in}$ [°C]	45.64
$\dot{Q}_{sink,max}$ [MW]	11.5
$A_{N,V}$ [Mio €]	3.92
$A_{N,B}$ [Mio €]	0.18
$A_{N,K}$ [Mio €]	1.09
A_N [Mio €]	5.2
PBP [a]	5
LCOH [€ · MWh^{-1}]	113

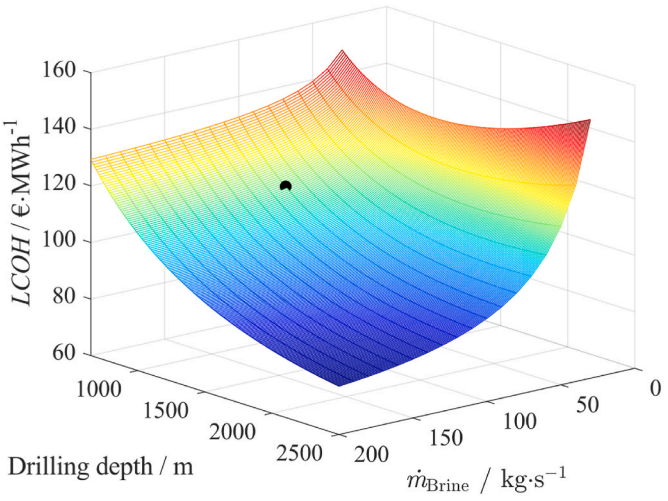

Fig. 8. LCOH as function of the drilling depth and thermal water mass flow, based on the modal values.

(geothermal gradient of the modal values). That means, that the *COP* is also increasing and the *LCOH* will decrease. The mass flow rate of the brine can vary from 30 kg/s up to 200 kg/s depending on the productivity of the borehole. As mentioned, the temperature difference of the thermal water supply and reinjection temperature is kept constant, so only the mass flow rate effects the thermal capacity. That leads to an increase of the *LCOH* at low mass flow rates and high drilling depths in fact of the high drilling costs.

Nevertheless, with a maximum of 150 €·MWh^{-1} at 2500 m drilling depth and a mass flow rate of 30 kg/s the project could be economically feasible, taking subsidies like the German subsidy program BEW [58] into account. With a mass flow rate above 80 kg/s and a drilling depth of 1690 m and above the *LCOH* are below 100 €·MWh^{-1}. An optimum can be found at the highest drilling depth of 2500 m and 200 kg/s and the economic and technical boundary conditions presented previously, with *LCOH* of 77 €·MWh^{-1}. Fig. 8 shows the enormous potential of the region under observation, with a wide range of *LCOH* below 100 €·MWh^{-1}, based on the modal values presented in Table 1. To account for the variability of the geothermal gradients in the SGMB, additionally to the modal values of Table 1, also the range from P10 to P90 values have to be considered. Fig. 9 presents the influence on the *LCOH* of the three cases (modal, P10, P90) with increasing drilling depth, at mass flow rate of 100 kg/s (please refer to Fig. 18 and 19 in the Appendix for the results for P10 and P90, for the whole mass flow rate range). While the P10 values represent a slightly higher geothermal gradient, resulting in a lower *LCOH*, the P90 values show a similar gradient at low depths. However, the model predicts a sharp drop in the depth of the reservoir, so that the strongly increasing capital related costs, as well as the increased electricity consumption of the ESP lead to different results compared to the other two models. Fig. 9 clarifies the necessity of utilising resilient geological models in techno-economic and ecological analyses for such complex energy systems. Nevertheless, the results of the models are in the same order of magnitude and also for P90 use cases an economic utilization may be possible.

As presented in Fig. 7, the demand related costs are the dominating cash flow and therefore have to be reduced to reduce the *LCOH*. So, in the following the electricity price is varied from 150 €·MWh^{-1} up to 350 €·MWh^{-1}. Fig. 10 shows a linear effect of the electricity price on the *LCOH*.

By reducing the electricity price to 150 €·MWh^{-1} the *LCOH* is reduced by 17 %, compared to the base scenario (black dot). Additionally, the Figure illustrates the influence of increasing full load hours on the *LCOH*. The trend shows an exponential behaviour and a reduction of 9.5 % of the *LCOH*, for an increase of the full load hours from 4000 h/a to 6000 h/a. In the following, the specific investment costs of the heat pump are varied, presented in Fig. 11. The specific investment costs are set to 500 €/kW thermal capacity of the heat pump, referring Arpagaus et al. [59]. The variation of the specific investment costs of the heat pump shows a positive effect on the *LCOH*. Reducing the specific costs from 500 €/kW to 250 €/kW, the *LCOH* can be reduced by up to 4 %. Additionally, the *COP* is varied from 2.5 up to a Carnot-*COP* of 70 %. The actual Carnot-*COP*s of heat pumps available on the market vary between 40 % and 60 %. So, the 70 % is used for an outlook resulting from more research and development in the future. As expected, the *LCOH* decrease with increasing *COP*. By an increase of the *COP* up to 55 % of the Carnot-*COP*, the *LCOH* can be reduced by up to 13 %. The presented results show that the boundary conditions have a great impact on the final evaluation of the application.

Using the proceeds of the first year, combined with the demand related costs, the capital value method is used to calculate the *PBP*. Fig. 12 presents the *PBP* as function of the drilling depth and mass flow rate, based on the modal values (please refer to Figure 20 and 21 in the Appendix for the results for P10 and P90, for the whole mass flow rate range) with the base scenario as a red dot.

A maximum occurs at the lowest mass flow rate and the highest drilling depth, caused by the small thermal capacity of 2.7 MW and quite

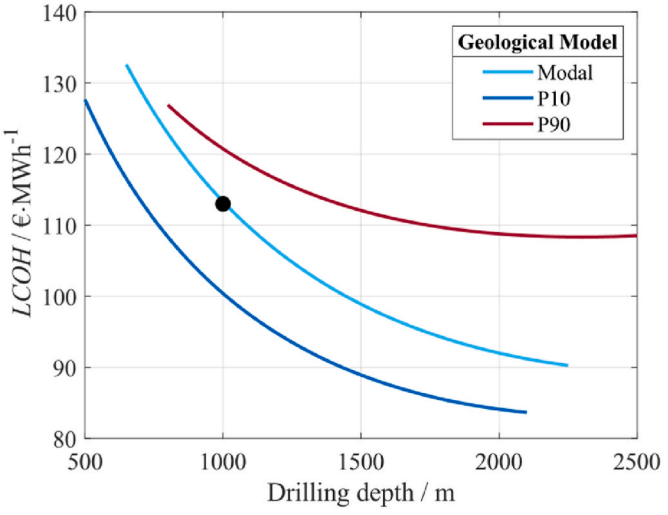

Fig. 9. LCOH as function of the drilling depth for different geological models, at $\dot{m}_{Brine}$ = 100 kg/s.

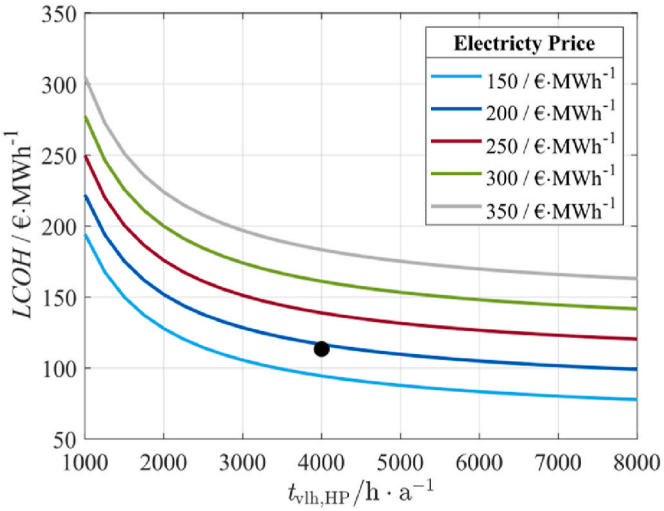

Fig. 10. LCOH as function of the electricity price and full load hours.

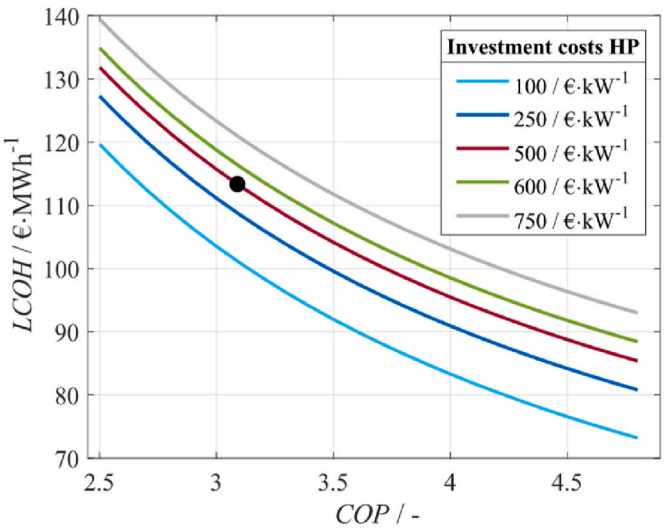

Fig. 11. LCOH as function of the specific investment costs of the heat pump and the COP.

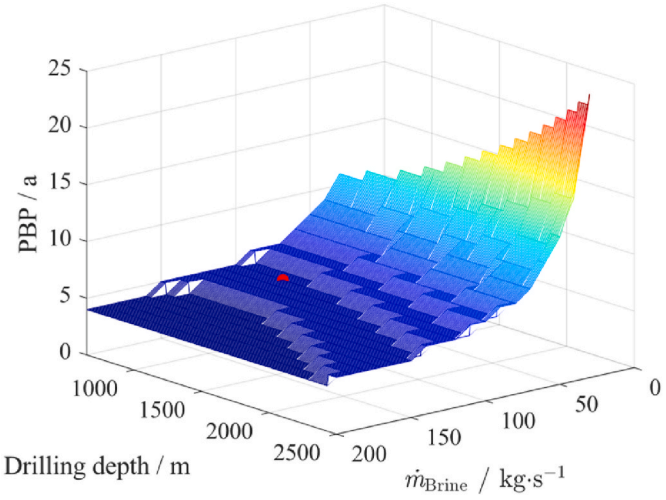

Fig. 12. PBP as function of the drilling depth and mass flow rate, based on the modal values.

high investment costs. When the mass flow rate reaches or exceeds 60 kg/s, the PBP remains at 10 years or less. The techno-economic analyses show the huge potential of the combination of medium-deep geothermal and large-scale heat pump. So, regions like the northern part of the SGMB could benefit from it and could help to increase the share of renewable heat sources, by realising viable projects.

4. Life cycle assessment

This chapter examines the environmental impact of medium-deep geothermal energy in the Southern German Molasse Basin coupled with large-scale heat pumps.

4.1. Fundamentals

In light of the Paris Climate Agreement, the environmental impact has become a prominent topic. Particularly within the energy sector, the building sector is responsible for 35 % in 2021 of energy related greenhouse gas emissions [60]. Given that, this sector is largely dominated by fossil fuels, there is a significant incentive to transition to renewable sources. To ascertain the environmental impact of a technology, it is essential to quantify its effects. The LCA method is a valuable tool for this purpose. The impact of conventional heat generation is thus quantified, thereby enabling the determination of avoidance factors—that is, the quantified amount of emissions avoided by replacing fossil energy technologies. Within the fossil mix, the most common heat source in Germany is natural gas [61]. The German Federal Environment Agency quantified the environmental impact of fossil and renewable sources as follows in Table 5.

As previously stated in the introduction, the EU Expert Group on Sustainable Finance [63] has established the threshold value of 100 g CO_2 eq./kWh that determines when the energy systems are in line with the Paris climate targets. Furthermore, the value declines by every five years until it reaches a net zero in 2050, thereby providing motivation for sustained efforts to provide a continued reduction. Upon examination of the potential heat sources in Tables 5 and it becomes evident that none of the fossil sources (as anticipated) can meet the specified limits. Even renewable sources do not consistently achieve the desired low values. While solar thermal energy, solid biomass, and the biogenic share of municipal waste, as well as deep geothermal energy, are usually below the threshold, there is some variation with the other sources, including liquid and gaseous biomass, and heat pumps.

For these reasons, it is imperative to undertake a more detailed examination of the system combination of medium-deep geothermal and large-scale heat pumps. While the emission factor for deep geothermal systems from the German Federal Environment Agency is quite low, with 36.4 g CO_2 eq/kWh, it is based on one specific heat plant and does not take into consideration the variation of geological boundary conditions or plant configurations. Lohse [64], for example, highlights the importance of reinjection to prevent pollution of surface water, further emphasizing the need to account for site-specific conditions when assessing the environmental impact of geothermal energy systems. Regarding different types of usage of the geothermal source, there is, for example, cogeneration of heat and electricity as well as sole heat generation. The cogeneration of electricity and heat has the advantage that the electricity produced in-house with a low *GWP* can cover its own requirements for the downhole pump and DHN pump, which has a positive influence on the *GWP* of heat generation, particularly in countries with an electricity mix with a high proportion of fossil fuels. For instance, Menberg et al. [65] reported a range of 3.9–4.0 g CO_2 eq./kWh for cogeneration plant in the Southern Molasse Basin. Similar values are obtained for a high temperature cogeneration plant in Iceland with 11.2–15.8 g CO_2 eq./kWh by Karlsdóttir et al. [66] as well as for a plant in the Upper Rhine Valley with 2.69–4.39 g CO_2 eq./kWh analysed by Pratiwi et al. [67].

On the other hand, the sole heat generation is heavily contingent upon the auxiliary energy employed. This shows parallels to the electrification of the heating sector due to the use of heat pumps. In the

Table 5
Emission factors for heat generation in Germany (2022) including direct and indirect emissions [62].

Energy source	Emission factor/g CO_2 eq•kWh^{-1}
Heating oil/diesel	312.7
Natural gas	257.0
Hard coal	432.7
Lignite briquettes	445.0
Solid biomass	10.6–25.1
Liquid biomass	4.5–143.8
Gaseous biomass	38.2–196.5
Biogenic share of municipal waste	1.3
Solar thermal	22.3–26.4
Shallow geothermal[a] and ambient heat[b] + heat pump	54.6–175.0
Deep geothermal	36.4

[a] Up to 400 m in depth.
[b] Including near-surface air layers and surface water.

context of the growing electrification of the heating sector, the electricity mix is becoming increasingly prevalent, exhibiting significant variations depending on the country of origin [68]. To illustrate, Douziech et al. [69] estimated a *GWP* of 3.8 g CO_2 eq./kWh for the French Rittershofen heat plant with the nuclear heavy French electricity mix, whereas Zhang et al. [70] did a feasibility study for a heat plant in China and obtain values of 187.7 g CO_2 eq./kWh due to the Chinese electricity mix being dominated by coal. For the value from the German Federal Environment Agency (see Table 5) 82.1 % of the emissions stem from auxiliary energy for the downhole pumps [62]. All of the aforementioned examples were situated within the deep geothermal range, where temperatures are sufficiently high to allow for the direct utilization of heat. In the case of lower temperature sources, namely those situated at shallow or medium depths, an increase in temperature is required, which in turn leads to an increase in electricity consumption. For example, the emissions for shallow geothermal sources coupled with heat pumps, are quantified by the German Federal Environment Agency with 163.2 g CO_2 eq./kWh from which 80,8 % are due to auxiliary energy use [62]. Pratiwi et al. [71] analysed medium-depth systems for heating and cooling in the State of Geneva in Switzerland and estimated 18.9 g CO_2 eq./kWh. Hereby, the district heating network was also considered, and the impact is dominated by the subsurface construction as the electricity mix is dominated by hydropower and therefore low *GWP*. Despite the growing interest in geothermal energy, medium-depth geothermal systems remain underrepresented in the existing LCA literature. Studies like those by Pratiwi et al. [71] have briefly examined this area, highlighting the need for more comprehensive research.

This study addresses a significant research gap by exploring the environmental aspects of integrating large-scale heat pumps into medium-depth geothermal energy systems, particularly while focusing on varying geological boundary conditions. The northern part of the Bavarian Molasse Basin serves as the case study for this analysis, as discussed in the previous chapters.

4.2. Methodology

The quantification of the environmental impact is carried out according to ISO 14044 [72] and 14040 [73]. Hereby, the LCA includes the four phases definition of goal and scope, inventory analysis, impact assessment and interpretation. This section describes these phases.

4.2.1. Definition of the goal and scope

The objective of this study is to conduct an LCA of hypothetical geothermal heating projects in the northern Molasse Basin including HPs, specifically covering medium deep wells. Thereby, significant influences and parameters on the environmental impact should be discovered. Additionally, the impact of the electricity mix is analysed. In the LCA, the life cycle phases of construction, operation, and decommissioning are considered for the major components and subsystems: two wells, one ESP and the HP. The boundary conditions are in line with the economic assessment as stated in Table 3. In particular, this includes a lifetime of 30 years, which is also in line with the boundary conditions for LCAs for geothermal systems proposed by Parisi et al. [74] and the maintenance work of exchanging the HP every 20 years as well as the ESP every seven years. A detailed LCI is provided in Table 10. The functional unit to which the environmental impact is related to is one kWh of heat at the plant.

4.2.2. Subsurface model

In order to cover different well depths a specific design for the injection and production well is considered (see Fig. 4). It is assumed that the wells are drilled straight down. For the first drill section (for the standtube), a length of 75 m is assumed. The length of the second section (anchor tube) is assumed to be 30 % of the total length (without open hole).

With regard to the production well, the third casing section is considered with an overlap of 75 m, and the injection well's third section is taken into account as a continuous pipe to the top edge. The specific weight for the three casing sections is listed in Table 6. The cementation is calculated based on the annulus. The respective amounts of cement and water per meter can be found in Table 6 as well as the amount of hydrochloric acid for the stimulation, drilling liquid and the energy demand for drilling covered by diesel. The composition of the drilling fluid can be found in Table 10 (Appendix). Additional to the construction of the wells, well heads and ESP and drill site preparation was considered.

4.2.3. HP model

For the HP a 5.25 MW system is considered which operates with the working fluid pentane. Thereby, the HP is scaled by power depending on the heat source (temperature and brine mass flow rate). It is assumed that the HP are connected parallelly to attain higher installed power levels.

4.2.4. Operation

For the operation of the heating plant the electricity demand is assumed in accordance to the consistent annual heat output (see Fig. 6). For the base scenario, it is assumed that the system is set into operation in 2024. Additionally, future changes in the German electricity mix are considered. Therefore, the development of the future German electricity mix from Flattler et al. [77] is used, specifically the "Start Scenario". Hereby, a reduction of the emission factor of 79 % from 2017 to 2050 is assumed. The average electricity mix over the lifetime from 2024 to 2054 as well as for the single years 2024 and 2054 is detailed in Table 7. Hereby the mix is created with processes from the ecoinvent database, whereas losses of network are considered.

4.2.5. Software and LCA impact assessment method

The LCA results are generated using the software SimaPro version 9.6.0.1 with the database ecoinvent version 3.10 [78]. As a system model, the allocation cut-off was selected. Parisi et al. [74] suggest guidelines for LCAs for geothermal energy generation in which they recommend using the method of environmental footprint [79]. Therefore, the newest version of the method 3.1 is used to generate results for

Table 6
Parameters of the subsurface LCI-model.

Parameter/unit	Value/Input
Casing 26"/kg•m^{-1}	191.9[a]
Casing 20"/kg•m^{-1}	139.9[b]
Casing 13 3/8"/kg•m^{-1}	90.8[b]
Cement type Section 1	CEM I 32.5[c]
Cement type Section 2 and 3	CEM III A 32.5 N[c]
Cementation Section 1 – cement/kg•m^{-1}	204.3[c]
Cementation Section 1 – water/kg•m^{-1}	89.9[c]
Cementation Section 2 – cement/kg•m^{-1}	107.2[c]
Cementation Section 2 – water/kg•m^{-1}	47.2[c]
Cementation Section 3 – cement/kg•m^{-1}	64.5[c]
Cementation Section 3 – water/kg•m^{-1}	49.7[c]
Stimulation HCl/kg well^{-1}	107.8[c]
Stimulation water/kg well^{-1}	251.5[c]
Stimulation energy/GJ well^{-1}	4.31[d]
Energy for drilling diesel/GJ m^{-1}	
<1500 m	1.6[e]
>1500	3.2[e]
Drilling liquid/kg•m^{-1}	
Section 1	72.2[b]
Section 2	287.2[b]
Section 3	486.3[b]

[a] Own calculations based on steel density of 7850 kg•m.^{3}.
[b] Information provided by drilling company.
[c] Information from medium-deep geothermal heating plant in the Southern German Molasse Basin.
[d] Based on Frick et al. [75].
[e] Based on Pratiwi et al. [76].

Table 7
Electricity mix for the years 2024, 2054 and the time period 2024–2054 according to [77].

Electricity source	Share/%		
	2024	2054	Average 2024–2054
Solar	8.7	13.7	11.9
Wind onshore	19.1	33.0	27.5
Wind offshore	7.5	22.6	15.3
Geothermal	0.9	0.8	0.9
Biomass	8.8	7.2	9.0
Hydro	3.6	3.2	3.8
Natural gas	16.5	17.6	17.7
Nuclear	7.7	0.0	2.8
Lignite	11.7	0.0	4.2
Hard coal	14.4	0.0	5.3
Pump storage	1.0	1.3	1.3
Lithium-ion battery	0.0	0.6	0.3

the environmental impacts. This method includes 16 impact categories which can be found in Table 8. Each in- and output of the Life cycle inventory (LCI_i) is multiplied by a respective characterisation factor provided by the database ecoinvent for each impact category Y (such as GWP) to quantify the environmental impact ($EI_{Y,i}$).

$$EI_{Y,i} = CF_Y \cdot LCI_i \tag{25}$$

To quantify the environmental impact of the complete System over the lifetime per functional unit ($EI_{\text{total,Y}}$), the environmental impact over the whole lifetime is summed up and divided by the total heat output ($Q_{lifetime}$).

$$EI_{\text{total,Y}} = \frac{\sum \left(EI_{Y,i}\right)}{Q_{lifetime}} \tag{26}$$

4.2.6. Boundaries

This study does not include a district heating network since the material demand is very dependent on the settlement and consumer structure. Additionally, in past studies the impact of the DHN plays only a minor role for the environmental impact [65]. Therefore, heat losses or additional electricity demand for the network pumps are not considered. Furthermore, infrastructure of peak load and redundancy is not included. Regarding the geological boundary conditions, the modal values from Table 1 are applied here.

4.3. Results

The general results for the base scenario for the different impact categories are listed in Table 9.

The environmental burden, detailed in the different impact categories are related to the total output of heat over the plant's lifetime. With a *GWP* of 103 g CO_2 eq./kWh the emissions are just shy of meeting the EU taxonomy's requirements of 100 g CO_2 eq./kWh [63]. Therefore, a closer look at the parameters that most influence the environmental burden makes sense. To illustrate the impact of the different impacts, in Fig. 13 the normalised results of the base scenario per impact category are depicted, detailing the subsurface components, HP general operation, and electricity consumption of the HP and ESP. Looking at the results it is apparent, that every impact category is dominated by the electricity consumption, especially concerning the operation of the HP. Which is commonly exhibited with heat pump systems as demonstrated by Violante et al. [80]. Additionally, the impact is due to the high fossil share in the German electricity mix of 27.2 % for the considered years 2024–2054 (see Table 9). Thereby, the impact of the electricity consumption of the HP ranges from 80 % (HTC) to 90 % (EF) and for the ESP from 7 % (HTC) to 8 % (EF). The construction and decommissioning of the plant components play only a minor role in the environmental burden, whereas the subsurface presents mostly as the biggest contributor in that selection. This is mainly due to the high environmental impact of the materials steel for the casing and the cementation, which make up 27.8 % and 42.2 % of the subsurface construction's *GWP* impact, respectively. The main impact on the construction of the HP is due to the frequency converter with 34.7 % of the *GWP* and the condenser with 24.7 %.

Table 8
Impact categories of the method EF 3.1 [79].

Impact category	Unit
Acidification (*AC*)	mol H+ eq
Climate change (*GWP*)	kg CO2 eq
Ecotoxicity, freshwater (*EFW*)	CTUe
Particulate matter (*PM*)	disease inc.
Eutrophication, marine (*EM*)	kg N eq
Eutrophication, freshwater (*EF*)	kg P eq
Eutrophication, terrestrial (*ET*)	mol N eq
Human toxicity, cancer (*HTC*)	CTUh
Human toxicity, non-cancer (*HTNC*)	CTUh
Ionising radiation (*IR*)	kBq U-235 eq
Land use (*LU*)	Pt
Ozone depletion (*OD*)	kg CFC11 eq
Photochemical ozone formation (*POF*)	kg NMVOC eq
Resource use, fossils (*RUF*)	MJ
Resource use, minerals and metals (*RUMM*)	kg Sb eq
Water use (*WU*)	m3 depriv.

Table 9
LCA results base scenario per kWh at the plant.

Impact category	Unit	Value
Acidification	mol H+ eq	$3.17 \cdot 10^{-4}$
Climate change	kg CO2 eq	$1.03 \cdot 10^{-1}$
Ecotoxicity, freshwater	CTUe	$5.05 \cdot 10^{-1}$
Particulate matter	disease inc.	$1.88 \cdot 10^{-9}$
Eutrophication, marine	kg N eq	$6.82 \cdot 10^{-5}$
Eutrophication, freshwater	kg P eq	$8.22 \cdot 10^{-5}$
Eutrophication, terrestrial	mol N eq	$6.15 \cdot 10^{-4}$
Human toxicity, cancer	CTUh	$4.13 \cdot 10^{-10}$
Human toxicity, non-cancer	CTUh	$1.58 \cdot 10^{-9}$
Ionising radiation	kBq U-235 eq	$8.13 \cdot 10^{-3}$
Land use	Pt	$6.24 \cdot 10^{-1}$
Ozone depletion	kg CFC11 eq	$2.21 \cdot 10^{-9}$
Photochemical ozone formation	kg NMVOC eq	$2.35 \cdot 10^{-4}$
Resource use, fossils	MJ	1.40
Resource use, minerals and metals	kg Sb eq	$1.55 \cdot 10^{-6}$
Water use	m3 depriv.	$1.05 \cdot 10^{-2}$

4.4. Sensitivity analyses

In this section, the influence of technical and location-based parameters is investigated with sensitivity analyses. In order to prevent an overload of information, the results are presented solely for the impact category *GWP*. The influence of the geological boundary conditions for brine mass flow rate and well depth is analysed for the *GWP* in Fig. 14 based on the modal values. The well depth and brine mass flow is varied analogous to the economic analysis from 650 m to 2500 m (excluding the additional 400 m open hole) and 30 kg/s - 200 kg/s for the mass flow rate of the brine.

As the well depth influences the thermal water temperature (see Equation (2)), the *COP* and thereby the electricity demand is influenced. Since the electricity demand is the single biggest influence on the *GWP*, the drilling depth and thereby the brine temperature shows a major influence on the *GWP* with a strong decrease with increasing well depth. On the other hand, the variation of the brine mass flow only shows a slight influence with a small decline of the *GWP* over the increasing mass flow. This is due to the *COP* remaining constant with the mass flow variation. These results are in contrast to the economical evaluation which also shows a big influence of the brine mass flow rate. Although it may not be financially feasible to operate plants at lower brine mass flow

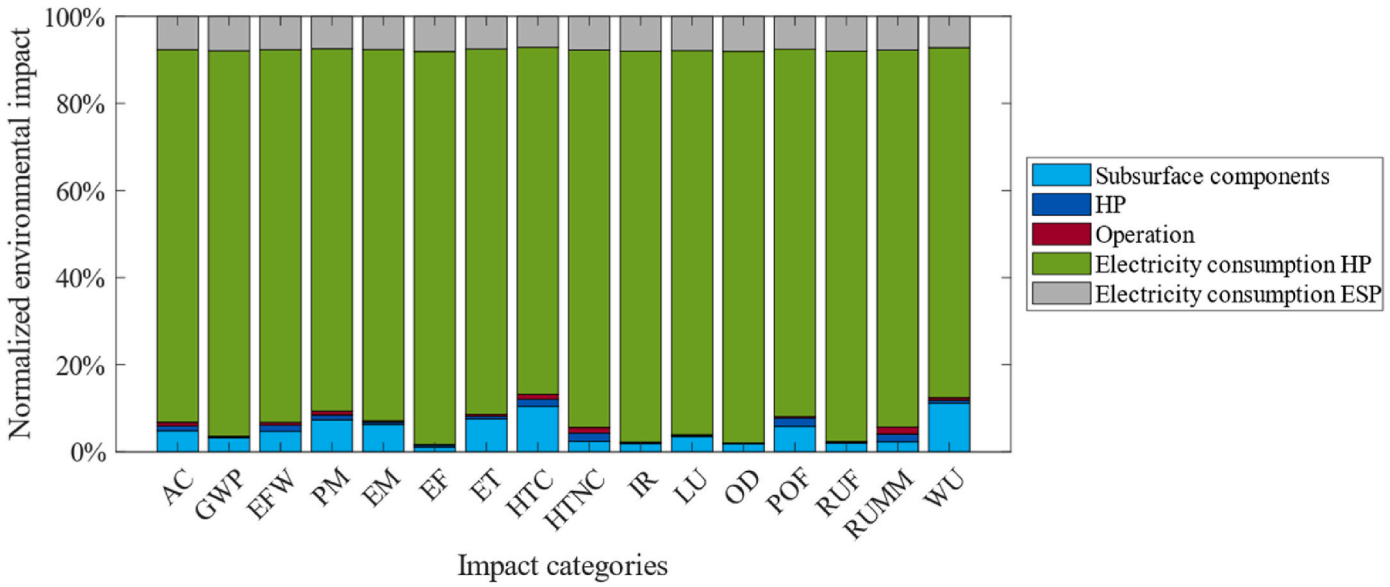

Fig. 13. Normalised LCA results of the base scenario.

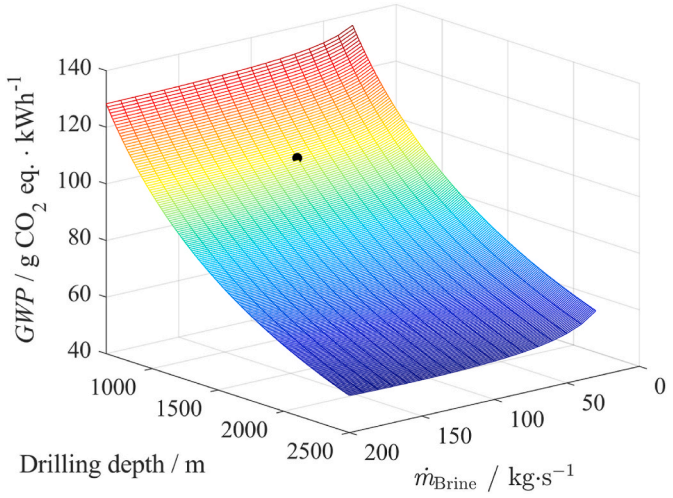

Fig. 14. GWP of the heating plant as function of the drilling depth and thermal water mass flow.

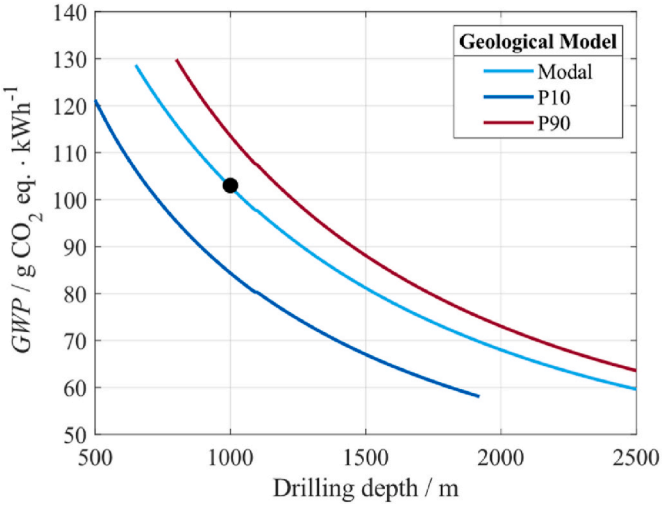

Fig. 15. GWP as function of the drilling depth for different geological models, at $\dot{m}_{Brine} = 100$ kg/s.

rates, from an ecological standpoint, these plants are a viable option as they predominantly remain below the 100 g CO_2 eq./kWh threshold for taxonomic classification. However, future policies concerning *GWP*, such as tax incentives, may potentially alter the viability of these plants. Looking at the overall results, it is apparent, that most of the configurations fall below the 100 g CO_2 eq./kWh threshold. At drilling depths >1200 m (at any brine mass flow rate) the *GWP* falls under the threshold. These results render most analysed systems as compatible with the Paris climate goals.

Since the relation between drilling depth and brine temperature is a distribution rather than fixed values (see Table 1, P10, modal values and P90) in the region of the Northern SGMB, this heterogeneity is mapped in Fig. 15. Hereby, next to the GWP of the modal values, the upper and lower percentiles P10 and P90 are also represented at a mass flow rate of 100 kg/s (please refer to Figure 22 and 23 in the Appendix for the results for P10 and P90, for the whole mass flow rate range). The P10 values with a higher geothermal gradient lead to lower GWPs since less additional energy for the HP is needed to reach the desired Temperatures for the DHN. All curves show a similar slope but the offset of P10 to the modal values is thereby bigger than the offset of the P90 values. In contrast to the economic assessment, the deviation of the P90 data behaves closer to the modal value. Meaning that even for less favourable conditions, on an environmental level, these systems are worthwhile. At depths lower than 1240 m (excluding the open hole), the *GWP* of P90 fall below the threshold value of 100 g CO_2 eq./kWh.

To investigate how the *GWP* is influenced by the electricity mix as well as the amount of full load hours and *COP* additional sensitivity analyses are conducted. In Fig. 16 the full load hours are varied from 1000 h/a - 8000 h/a to demonstrate the influence of different capacity utilization and customers. Additionally, since for the base scenario the electricity consumption has proven to have a major impact, the *GWP* of the electricity mix is varied from 50 g CO_2 eq./kWh_{el} to 500 g CO_2 eq./kWh_{el}. The base scenario is highlighted as black dot on the red curve. In contrast to the economic evaluation (see Fig. 10), the amount of full load hours only has a minor influence. There is only a slight downturn of the graph with the increase of full load hours. These results are to be expected since the ratio of consumed electricity to heat, determined by the *COP* of the HP, stays consistent. This flattens the curve since electricity consumption is the main contributor. The impact of the plant's

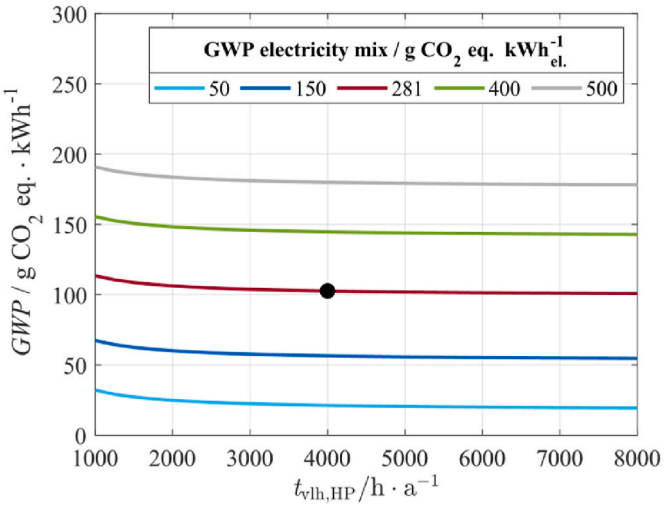

Fig. 16. GWP of the heating plant as a function of the GWP of the consumed electricity mix and full load hours.

construction maintenance and decommissioning is responsible for the slight decrease because it is constant independent of the full load hours. Hence, with increasing heat output, the *GWP* decreases. The *GWP* of the electricity mix however has a much greater influence. The values greater than the base scenario would usually be associated with fossil electricity generation.

At 4000 full load hours with an electricity mix around 400 g CO_2 eq./kWh_{el} and 500 g CO_2 eq./kWh_{el}, which are conditions similar to the fossil heavy electricity mix in Poland, the *GWP* of the heat generation lays at 144 g CO_2 eq./kWh_{el} and 180 g CO_2 eq./kWh which is far above the EU's taxonomy threshold of 100 g CO_2 eq./kWh_{el} [63]. On the other hand, the lower *GWP* electricity mixes decrease the impact significantly with 56 g CO_2 eq./kWh_{el} (for 150) and 21 g CO_2 eq./kWh (for 50), falling way below the threshold. These results are especially important since the threshold decreases every five years until net zero in 2050 [63]. This highlights the importance of transitioning to renewable sources for the electricity sector. Fig. 17 depicts the influence of the *COP* as well as the *GWP* of the electricity mix. As expected with increasing *COP* the *GWP* decreases analogous to the *LCOH* in the economic evaluation (see Fig. 11).

As the main influence, the electricity consumption is reduced with

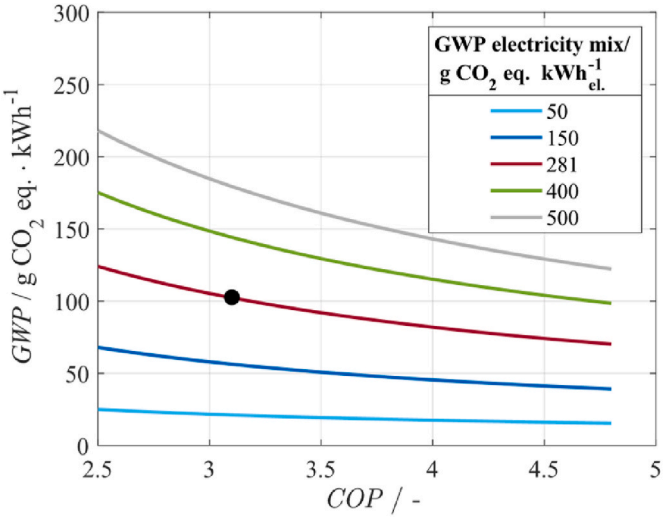

Fig. 17. GWP of the heating plant as function of the GWP of the consumed electricity mix and the COP.

the increase of the *COP*. For the base scenario (red line) the variation of the *COP* leads to a decrease in *GWP* of 48 % from 124 g CO_2 eq./kWh at a *COP* of 2.5–70 g CO_2 eq./kWh_{el} at a *COP* of 4.8. Similar to the full load hour sensitivity analysis, the electricity mix again has a mayor influence on the results although the impact of the *COP* is much greater than that of the full load hours. With decreasing electricity mix *GWP* the influence on the impact lessens - the reduction potential of the *COP* decreases with 44 % at 500 g CO_2 eq./kWh_{el} to 38 % at 50 g CO_2 eq./kWh_{el} as seen in the flattening of the curves. At an electricity mix *GWP* of 500, at the lowest *COP* of 2.5, the *GWP* for heat generation reaches the maximum value of 218 g CO_2 eq./kWh. To set this into perspective, this *GWP* even exceeds to caloric value based *GWP* of natural gas with 202 g CO_2 eq./kWh [81]. With an electricity mix *GWP* greater than 400 g CO_2 eq./kWh_{el} the EU taxonomy threshold value of 100 g CO_2 eq./kWh [63] can only be reached at very high *COP*s > 4.7. Therefore, it can be concluded that a high *GWP* electricity mix can only be compensated to a limited extent through technological improvement.

On the other hand, the minimum *GWP* of 15 g CO_2 eq./kWh is obtained with the lowest *GWP* electricity mix at 50 g CO_2 eq./kWh_{el} as well as the highest analysed *COP* of 4.8. This value is even comparable to deep geothermal heat projects which use mostly renewable electricity mixes: A case study of a hypothetical geothermal plant in Scotland shows similarly low results with 9.7 g CO_2 eq./kWh_{el} to 14.0 g CO_2 eq./kWh [82]. These sensitivity analyses show that even for systems with higher *GWP*, the values could be lowered with different electricity mixes or technical improvements to increase the *COP* (see Fig. 17).

5. Conclusion

Next to the north German basin and the Upper Rhine Plain, the South German Molasse Basin is one of three major hydrothermal reservoirs in Germany. The presented study investigates the utilization of the medium deep northern part of the Molasse Basin by integration of large-scale heat pumps for district heating at a supply temperature level of 100 °C. Based on the few borehole data in the region, literature and free available geological data, the key parameters of the reservoir were defined. Taking the depth of top reservoir, reservoir thickness, production temperature, and production rate into account, the design of large-scale heat pumps was conducted. Following, a base scenario was defined, taking a top reservoir depth of 1000 m and a mass flow rate of 100 kg/s into account. The base scenario leads to *LCOH* of 113 €·MWh^{-1} and a *PBP* of 5 years, based on a system *COP* (electrical power consumption of heat pump and *ESP* considered) of 2.84. To evaluate the impact of different boundary conditions on the results, sensitivity analyses were used. Following parameters were varied with the stated boundaries.

- Electricity price [150–350 €·MWh^{-1}]
- Full load hours [1000–8000 h/a]
- Investment costs HP [100–750 €/kW]
- *COP* [2.5–70 % Carnot-*COP*]
- Drilling depth [650–2500 m]
- Mass flow rate [30–200 kg/s]
- Temperature gradient [P10 – P90 from Table 1]

The reduction of the electricity price from 192 €·MWh^{-1} to 150 €·MWh^{-1} leads to a decrease of 17 % in the *LCOH*. By increasing the *COP* up to 55 % of the Carnot-*COP*, the *LCOH* can be reduced by up to 13 %. By varying the drilling depth, combined with the variation of the mass flow rate, the *LCOH* can be calculated for every possible combination occurring in the investigated region. With a minimum of the *LCOH* at 2500 m and 200 kg/s of 77 €·MWh^{-1} and a maximum at the same depth and 30 kg/s of 150 €·MWh^{-1}. Additional to the economic analysis, the environmental impact via LCA was analysed. Thereby the construction of wells of different depths, HPs with different installed capacities, operation with replacement of the ESP and HP, and their electricity

requirements covered by the time dependent German electricity mix over the years 2024–2054 were considered. Finally, the decommissioning of the system is considered as well. For the base scenario, 16 impact categories of the EU Environmental Footprint method were calculated. The most significant impact in all impact categories is related to the electricity demand of the HP. This aspect is reinforced by environmental impact of the German electricity mix with an average *GWP* of 281 g CO_2 eq./kWh_{el}. To sum up, the *GWP* of the base scenario is 103 g CO_2 eq./kWh which is marginal over the threshold value of 100 g CO_2 eq./kWh which is defined by the EU's Expert Group on Sustainable Finance as in line with the Paris Climate Agreement. Technical improvements in heat pump technology, a faster expansion of the energy transition or favourable geological conditions can easily meet the stated target value of 100 g CO_2 eq./kWh. This is illustrated by the sensitivity analyses carried out to investigate the influence of certain boundary conditions on the *GWP* of the System. Analogous to the economic evaluation the full load hours, *COP*, drilling depth and mass flow rate were varied. Additionally, the *GWP* of the electricity mix was analysed with a value range of 50–500 g CO_2 eq./kWh_{el}. While the full load hours show near to no influence on the *GWP*, with the reduction of the *COP* the base scenario can be reduced by 43 %. The biggest influence however is the electricity mix. With a electricity mix *GWP* of 50 CO_2 eq./kWh_{el} and a *COP* of 4.8 a minimum of 15.5 g CO_2 eq./kWh could be reached. When varying the geological boundaries drilling depth and mass flow rate, it was evident that mainly the drilling depth influences the impact. The mass flow rate plays a minor role. An increase in drilling depth as well as mass flow rate decreases the *GWP*. Generally, at depths exceeding 1200 m the *GWP* falls below the threshold of 100 g CO_2 eq./kWh. Thereby proving the alignment of these medium-depth systems with the Paris Climate Agreement.

The present study thus offers a comprehensive and holistic analysis of the geothermal potential in the northern SGMB and its utilization through the integration of large-scale heat pumps. Pan et al. [83] present approaches to overcoming barriers to the implementation of enhanced geothermal systems within existing energy systems. Some of these barriers are transferable to the use case examined in this study, and the findings contribute to addressing certain challenges identified by Pan et al. [83]. Especially the lack of expertise within community/city government and the lack of exploration data can be addressed in the presented study. Even without subsidies, the establishment of such a heating plant is recommended for both economic and ecological reasons across large parts of the study region. Consequently, even smaller municipalities within the study region can conduct an initial assessment to determine whether the ecological and techno-economic conditions provide a suitable basis for a feasibility study. This can facilitate the removal of obstacles and further promote the decarbonization of the heating sector.

5.1. Limitations of the workflow and uncertainties

In this section, occurring uncertainties are described and discussed. Concerning the geological boundary conditions, key parameters are the temperature of the produced water and the flow rate. Since there is a lack of empirical data for the northern SGMB, both parameters had to be roughly estimated or derived from the larger data set available for the southern SGMB from deep boreholes. The fluid temperatures were derived from a correlation (Zosseder et al. [9]) of outflow temperatures of the southern SGMB geothermal wells versus the undisturbed formation temperatures at top Malm from the 3D temperature model GeotIS (Agemar et al. [19,20]). As the GeotIS temperatures are mainly based on error-prone corrections of low quality bottom hole temperatures (e.g., Schölderle et al. [84]) and the spatial prognosis of the temperature values is generally subject to an uncertainty (Agemar et al. [19]), the estimated production temperature should be considered in the context of these uncertainties. The flow rates in this study were estimated conservatively with a high uncertainty range of 30–200 kg/s in order to reflect the heterogeneous conditions of the reservoir, which are known from the southern part of the SGMB (Zosseder et al. [9]). It is unclear to what extent these conditions can be applied to the northern part. Although the well-known north-south depth porosity trend indicates good hydraulic conditions (Zosseder et al. [9]), the possible hydraulic influence of the absence of the Purbeck formation in the north has not yet been thoroughly investigated. Lastly, the high reservoir depths (>2000 m) can largely be found in the negative temperature anomaly east of Munich, in the Wasserburg Through, which is known to bear lower thermal gradients (e.g. Agemar et al. [19], Przybycin et al. [21]). At these depths, the applied well scheme (Fig. 4) is not tenable, and an additional well section would be needed to obtain the necessary drilling mud pressures during production of the boreholes. The uncertainties and limits in the techno-economic analyses can be identified in the thermodynamic simulation and economic boundary conditions. So, the assumed *COP* could be calculated using an extensive simulation model. The installation depth of the ESP is also one uncertainty and would infect the system *COP*. The economic boundary conditions show a snapshot of the situation and has to be varied focusing on other regions or periods of observation. Concerning the LCI model of the wells the material input for the creation of the wells is, by definition, an estimation. In principle, an attempt is made to assume a realistic input, generally on the conservative side. The well and casing design is highly sight-specific and cannot be generalized. Especially, for higher depths the sections would generally be smaller, and an additional section could be included (thereby the input would be smaller per m). When considering the future electricity mix only current *GWP*s for the different technology are considered. As technology advances, it is likely that the environmental impact will be reduced, although it is challenging to make an accurate estimation of this. This will have a positive effect on the performance of the HP system. Regarding the considered HP, particularly for installed power values that are less than the considered HP with 5.25 MW, the estimation is accompanied by a certain degree of uncertainty. It is likely that smaller HP are not estimated correctly by a fraction of a bigger dimensioned one. Furthermore, only a single specific HP was considered by using natural refrigerant as working fluid. If this were not the case, the environmental impact could increase, although it is estimated to still play a minor role compared to the impact of the electricity mix. In the definition of the boundaries, peak load and redundancy were not considered. In many cases this demand is covered by natural gas or heating oil boilers, which in their fossil nature, would have negative effects on the environmental impact. There could, however, be additional HPs used for peak load, which would require additional design and optimization.

Overall, the specific results cannot be transferred directly into other geological regions, since the geological boundary conditions require different drilling technologies and the temperature gradient as well as the thermal water mass flow is always very reservoir specific. However, the workflow and the techno-economic and ecological calculations can be transferred and conducted for other regions and reservoirs.

CRediT authorship contribution statement

J. Jeßberger: Writing – review & editing, Writing – original draft, Visualization, Validation, Methodology, Investigation, Formal analysis, Data curation, Conceptualization. **H. Uhrmann:** Writing – review & editing, Writing – original draft, Visualization, Validation, Methodology, Investigation, Formal analysis, Data curation, Conceptualization. **F. Schölderle:** Writing – review & editing, Writing – original draft, Visualization, Validation, Methodology, Investigation, Formal analysis, Data curation. **D. Pfrang:** Writing – review & editing, Writing – original draft, Validation, Methodology, Investigation, Formal analysis, Data curation, Conceptualization. **F. Heberle:** Writing – review & editing, Supervision, Conceptualization. **K. Zosseder:** Writing – review & editing, Supervision, Funding acquisition, Conceptualization. **D. Brüggemann:** Supervision, Funding acquisition.

Acknowledgment and funding sources

We gratefully acknowledge the Bavarian State Ministry of Science and Arts within the framework of the "Geothermal Alliance Bavaria" project for funding.

Funded by the Deutsche Forschungsgemeinschaft (DFG, German Research Foundation) – 491183248. Funded by the Open Access Publishing Fund of the University of Bayreuth.

We also thank the geothermal energy planning office Erdwerk GmbH for the kind exchange about likely drilling and well designs in the not yet utilized shallower part of the study area.

Declaration of competing interest

The authors declare that they have no known competing financial interests or personal relationships that could have appeared to influence the work reported in this paper.

Nomenclature

a	annuity factor, -	r_x	annual increase of c_x, -
A_x	annuity of x, €·a^{-1}	T	temperature, °C
BS	bitsize, in	t_{fl}	full load hours, h·a^{-1}
b_x	price dynamic value factor, -	$\dot{V}$	volume flow rate, m^3·s^{-1}
CF_Y	characterisation factor for the impact category Y	w	flow velocity, m·s^{-1}
COP	coefficient of performance, -	Δp_v	pressure losses, MPa
c_w	volumetric heat capacity, MJ·m^{-3}·K^{-1}	ε	tube roughness, mm
c_x	costs for x, €	η	dynamic viscosity, Pa·s
d	standpipe diameter	η_{elec}	pump efficiency, -
E	proceeds, €·a^{-1}	λ	tube friction coefficient, -
$EI_{total,Y}$	environmental impact of the complete System over the lifetime per functional unit for the impact category Y	ρ	density, kg·m^{-3}
$EI_{Y,i}$	environmental impact for the impact category Y and input i	***Abbreviations***	
f_{inst}	factor for maintenance, -	DHN	District heating network
$f_{m\ +\ insp}$	factor for servicing and inspection, -	EF	Eutophication, freshwater
GWP	Global warming potential, g CO_2 eq. kWh^{-1}	ESP	Electronic submersible pump
H	pump head, m	HP	Heat pump
ID	inner diameter, in	HTHP	High-temperature heat pump
K	capital value, €	HTC	Human toxicity, cancer
L	tube length, m	LCA	Life cycle assessment
LCI_i	life cycle inventory input i	LCI	Life cycle inventory
$LCOH$	levelized costs of heat, €·kWh^{-1}	SGMB	South German Molasse Basin
OD	outer diameter, in	sink	Heat sink of the heat pump
P	power, W	source	Heat source of the heat pump
p	pressure, MPa	TVD	True Vertical Depth
PBP	payback period, a		
q	interest rate, -		
Q	heat demand, kWh·a^{-1}		
$\dot{Q}$	thermal capacity, kW		
$Q_{lifetime}$	Heat output over the lifetime		
Re	Reynolds number, -		

Appendix

Sensitivity Analyses

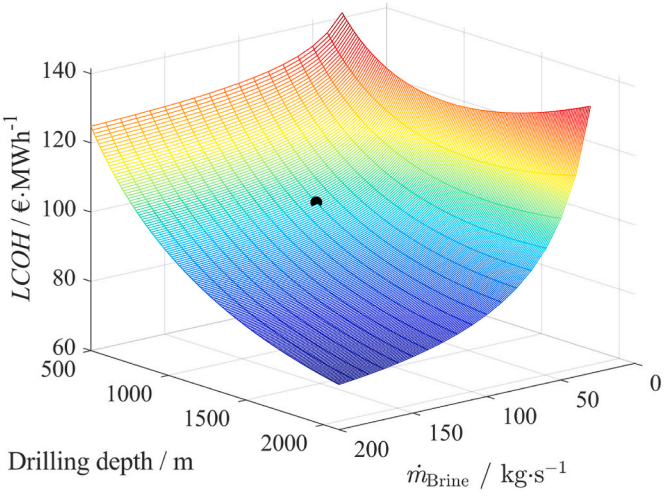

Fig. 18. LCOH as function of the drilling depth and thermal water mass flow, based on geothermal gradient P10.

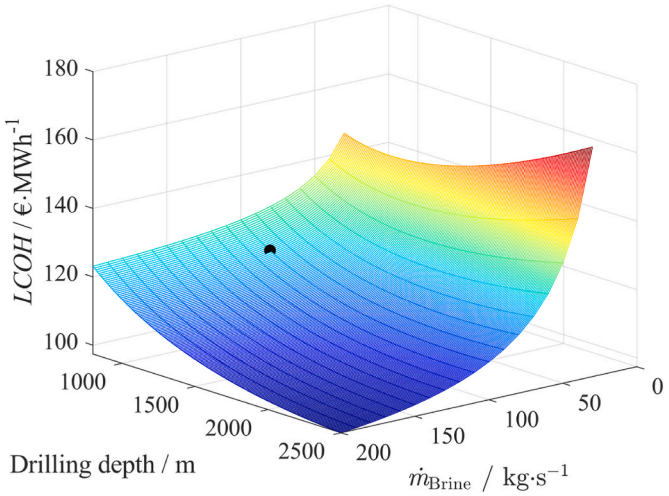

Fig. 19. LCOH as function of the drilling depth and thermal water mass flow, based on geothermal gradient P90.

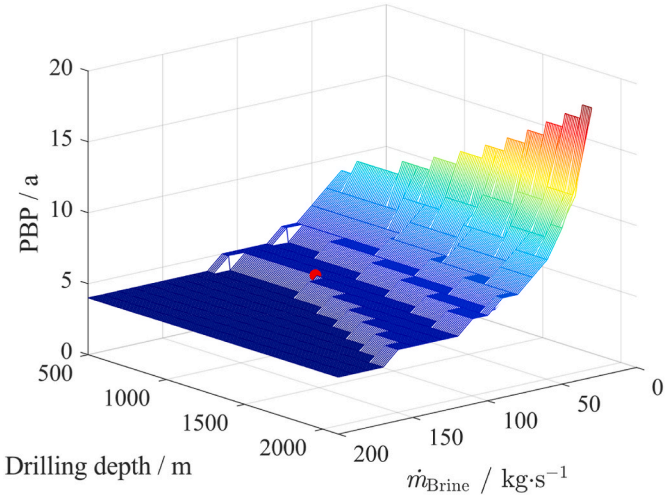

Fig. 20. PBP as function of the drilling depth and mass flow rate, based on geothermal gradient P10.

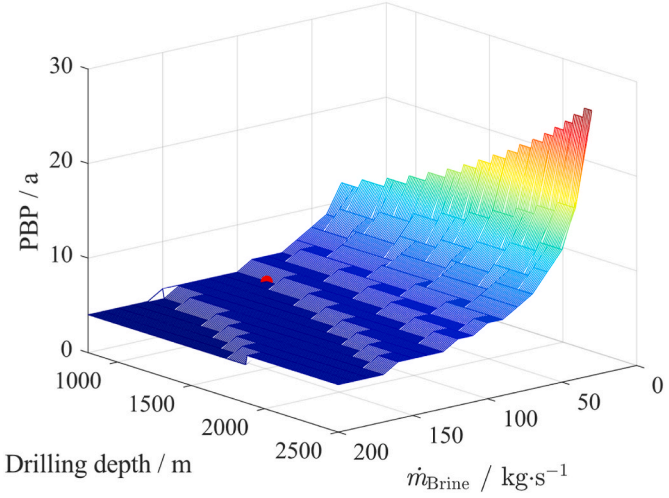

Fig. 21. PBP as function of the drilling depth and mass flow rate, based on geothermal gradient P90.

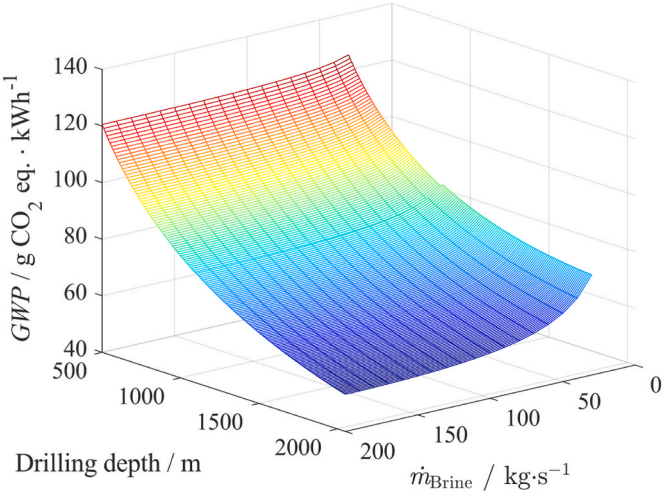

Fig. 22. GWP as function of the drilling depth and thermal water mass flow, based on geothermal gradient P10.

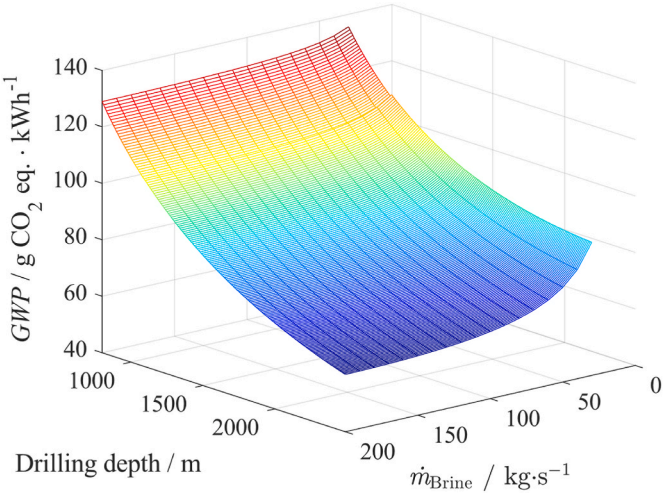

Fig. 23. GWP as function of the drilling depth and thermal water mass flow, based on geothermal gradient P90.

8.2. LCI

Table 10
Supplementary LCI to Table 6 for the subsurface construction

Parameter	Description	Unit	Value	Source
Construction subsurface				
Drilling site preparation	Cement, unspecified	kg/well	300	Frick et al. [75]
	Diesel, burned in building machine	MJ/well	20000	Frick et al. [75]
Drilling rig drive	Diesel in construction equipment	GJ	12431	operator
Geothermal fluid cycle	DHN pipes DN250 installed in urban area	m	4300	operator
Deep well pump	Steel, low-alloyed and metal working	kg	1224	operator, Frick et al. [75]
	Steel, chromium steel 18/8 and metal working	kg	10927	operator, Frick et al. [75]
	Aluminium bronze and metal working	kg	2449	operator, Frick et al. [75]
	Transport, freight, lorry 16–32 metric ton, euro3	tkm	9490	operator
Well casing	Steel, chromium steel and drawing of pipes	kg	$1/3 \bullet m_{steel}$[a]	Frick et al. [75]
	Steel, low-alloyed and drawing of pipes	kg	$2/3 \bullet m_{steel}$[a]	Frick et al. [75]
	Drawing of pipe, steel	kg	m^{a}_{steel}	Frick et al. [75]
Reservoir enhancement	Diesel, burned in diesel-electric generating set	GJ/well	4.31	Frick et al. [75]
Well head	Steel, low-alloyed and metal working	t	14.9	operator
Drilling fluid section 1	Bentonite	kg/m	2.861	Drilling company
	Carboxymethyl cellulose	kg/m	0.351	Drilling company
	Soda ash	kg/m	0.176	Drilling company
	Barite	kg/m	67.882	Drilling company
	Citric acid	kg/m	0.520	Drilling company

(*continued on next page*)

Table 10 (*continued*)

Parameter	Description	Unit	Value	Source
	Silica sand	kg/m	0.039	Drilling company
	Sodium bicarbonate	kg/m	0.260	Drilling company
	Tap water	kg/m	0.149	Drilling company
Drilling fluid section 2	Barite	t/m	0.182	Drilling company
	Bentonite	t/m	0.000	Drilling company
	Quicklime	t/m	0.041	Drilling company
	Calcium carbonate	t/m	0.001	Drilling company
	Citric acid	t/m	0.003	Drilling company
	Potassium carbonate	t/m	0.036	Drilling company
	Chemical, organic	t/m	0.001	Drilling company
	Sugar, from sugar beet	kg/m	0.027	Drilling company
	Carboxymethyl cellulose, powder	t/m	0.006	Drilling company
	Polyacrylamide	t/m	0.001	Drilling company
	Fatty acid methyl ester	t/m	0.000	Drilling company
	Soda ash	kg/m	0.007	Drilling company
	Cellulose fibre	kg/m	0.007	Drilling company
	Sodium bicarbonate	t/m	0.000	Drilling company
Drilling fluid section 3	Barite	t/m	0.408	Drilling company
	Bentonite	kg/m	0.038	Drilling company
	Quicklime	t/m	0.043	Drilling company
	Naphthalene sulfonic acid	kg/m	0.253	Drilling company
	Citric acid	t/m	0.001	Drilling company
	Urea	t/m	0.001	Drilling company
	Potassium carbonate	t/m	0.011	Drilling company
	Chemical, organic	t/m	0.001	Drilling company
	Cellulose fibre	t/m	0.004	Drilling company
	Sugar, from sugar beet	t/m	0.025	Drilling company
	Polyacrylamide	kg/m	0.431	Drilling company
	Carboxymethyl cellulose, powder	t/m	0.003	Drilling company
Transport subsurface	Transport, freight, lorry >32 metric ton	tkm	288000	Frick et al. [75]
	Transport, freight train	tkm	826000	Frick et al. [75]
Operation				
Exchange downhole pump		/	4	
Decommissioning				
	Well closure	m	Well depth	

[a] mass of steel dependent on drilling depth see Table 6, steel type according to Frick et al. [75].

Table 11
LCI for the heat pump

Parameter	Description	Unit	Value	Source
Construction				
metals	Steel, chromium steel and metal working	kg	5875.46	HP manufacturer
	Steel, low-alloyed and metal working	kg	9974.16	HP manufacturer
	Copper and metal working	kg	2264.44	HP manufacturer
	Cast iron and metal working	kg	1069.24	HP manufacturer
	Aluminium and metal working	kg	1752.32	HP manufacturer
	Electronics, for control units	kg	560.59	HP manufacturer
	Brass and metal working	kg	21.12	
Plastics	Stone wool	kg	381.6	HP manufacturer
	Polyvinylchloride	kg	71.04	HP manufacturer
	Polyethylene	kg	71.04	HP manufacturer
	Polyethylene terephthalate	kg	18.04	HP manufacturer
	Synthetic rubber	kg	47.36	HP manufacturer
	Acrylonitrile-butadiene-styrene copolymer	kg	6	HP manufacturer
	Polypropylene	kg	6	HP manufacturer
	Nylon 6-6	kg	12.04	HP manufacturer
	Polycarbonate	kg	54.16	HP manufacturer
Working fluid	Pentane	kg	4480	HP manufacturer
Lubricant	Lubricating oil	kg	960	HP manufacturer
Transport	Transport, freight, sea, ferry	tkm	491.52	HP manufacturer
	Transport, freight, lorry, unspecified	tkm	41987.21	HP manufacturer
	market for transport, freight, lorry >32 metric ton EURO4	tkm	25100	HP manufacturer
Energy	Electricity	kWh	200.18	HP manufacturer
	Heat, district or industrial, natural gas	MJ	14979.86	HP manufacturer
Operation	Pentane leakage	kg	3081.12	HP manufacturer
Decomissioning	Waste mineral wool	kg	381.6	HP manufacturer
	Waste polyvinylchloride	kg	71.04	HP manufacturer
	Waste polypropylene	kg	6	HP manufacturer
	Waste plastic mixture	kg	72.2	HP manufacturer
	Waste polyethylene	kg	18.04	HP manufacturer

(*continued on next page*)

Table 11 (*continued*)

Parameter	Description	Unit	Value	Source
	Waste rubber	kg	53.36	HP manufacturer
	Electronic scrap	kg	560.59	HP manufacturer
	Scrap steel	kg	2586.291	HP manufacturer
	Scrap copper	kg	452.888	HP manufacturer
	Hazardous waste	kg	644	HP manufacturer
	Aluminium scrap	kg	908.854	HP manufacturer

References

[1] European Union, Renewable energy for heating & cooling up to 25% in 2022. https://ec.europa.eu/eurostat/web/products-eurostat-news/w/ddn-20240227-2#:~:text=Energy%20for%20heating%20and%20cooling,)%20from%202021%20(23.0%25, August 20, 2024.

[2] Geothermal Alliance Bavaria - GAB, Standortkarte. https://geothermie-allianz.de/standortkarte/, March 19, 2025.

[3] G. Jia, Z. Ma, Z. Zhang, J. Hao, Y. Cao, Y. Ma, et al., Thermal performance and influencing range of underground inclined medium-deep geothermal heat exchangers, Renew. Energy 243 (2025) 122619, https://doi.org/10.1016/j.renene.2025.122619.

[4] H. Semmari, F. Bouaicha, S. Aberkane, A. Filali, D. Blessent, M. Badache, Geological context and thermo-economic study of an indirect heat ORC geothermal power plant for the northeast region of Algeria, Energy 290 (2024) 130323, https://doi.org/10.1016/j.energy.2024.130323.

[5] Y. He, M. Jia, X. Li, Z. Yang, R. Song, Performance analysis of coaxial heat exchanger and heat-carrier fluid in medium-deep geothermal energy development, Renew. Energy 168 (2021) 938–959, https://doi.org/10.1016/j.renene.2020.12.109.

[6] S. Dong, Y. Yu, B. Li, L. Ni, Thermal analysis of medium-depth borehole heat exchanger coupled layered stratum thermal conductivity, Renew. Energy 246 (2025) 122880, https://doi.org/10.1016/j.renene.2025.122880.

[7] R. Kiran, R. Upadhyay, V.K. Rajak, A. Kumar, S. Datta Gupta, Underpinnings of reservoir and techno-economic analysis for himalayan and Son-Narmada-Tapti geothermal sites of India, Renew. Energy 237 (2024) 121630, https://doi.org/10.1016/j.renene.2024.121630.

[8] Energieverbrauch für fossile und erneuerbare Wärme, Dessau-Roßlau (2024). https://www.umweltbundesamt.de/daten/energie/energieverbrauch-fuer-fossile-erneuerbare-waerme.

[9] C. Zhu, C. Quan, P. Shi, B. Li, J. Zhang, M. Li, Analysis and optimization of a medium-depth ground source heat pump heating systems with heat storage and borehole heat exchangers, Energy Rep. 11 (2024) 1455–1471, https://doi.org/10.1016/j.egyr.2024.01.022.

[10] X. Wang, T. Zhan, G. Liu, L. Ni, A field test of medium-depth geothermal heat pump system for heating in severely cold region, Case Stud. Therm. Eng. 48 (2023) 103125, https://doi.org/10.1016/j.csite.2023.103125.

[11] Bayerische Staatsregierung, Verordnung Zur Änderung Der Verordnung Zur Ausführung Energiewirtschaftlicher Vorschriften: Baygvbl. Nr. 24/2024, 2024.

[12] I. Stober, K. Bucher, Geothermal Energy, Springer International Publishing, Cham, 2021.

[13] R. DiPippo (Ed.), Geothermal Power Generation: Developments and Innovation, Elsevier WP, Amsterdam [u.a.], 2016.

[14] K. Zosseder, D. Pfrang, F. Schölderle, D. Bohnsack, F. Konrad, Characterisation of the Upper Jurassic geothermal reservoir in the South German molasse basin as basis for a potential assessment to foster the geothermal installation development – results from the joint research project geothermal alliance Bavaria, Geomech. Tunnelling 15 (1) (2022) 17–24, https://doi.org/10.1002/geot.202100087.

[15] J. Birner, Hydrogeologisches Modell Des Malmaquifers Im Süddeutschen Molassebecken [Dissertation], Freie Universität Berlin, Berlin, 2013.

[16] F. Böhm, Die Lithofazies Des Oberjura (Malm) Im Großraum München Und Deren Einfluss Auf Die Tiefengeothermische Nutzung [Dissertation], Freie Universität Berlin, Berlin, 2012.

[17] D. Bohnsack, K. Zosseder, M. Potten, H. Kaesling, K. Thuro, Geomechanical Investigation of a Geothermal Aquifer in the South German Molasse Basin, 2019.

[18] G.H. Bachmann, M. Müller, K. Weggen, Evolution of the molasse basin (germany, Switzerland), Tectonophysics 137 (1–4) (1986) 77–92, https://doi.org/10.1016/0040-1951(87)90315-5.

[19] M. Keim, T. Hamacher, M. Loewer, A. Molar-Cruz, C. Schifflechner, K. Zosseder, M. C. Drews, T. Ferrand, C. Wieland, P. Kuhn, W. Bauer, D. Bohnsack, F. Heine, F. Konrad, D. Pfrang, F. Schölderle, Bewertung masterplan geothermie, Munich (2020).

[20] T. Agemar, R. Schellschmidt, R. Schulz, Subsurface temperature distribution in Germany, Geothermics 44 (2012) 65–77, https://doi.org/10.1016/j.geothermics.2012.07.002.

[21] T. Agemar, 3D subsurface temperature model of Germany and Upper Austria. Compilation of gridded data (25 MB) and documentation, Available from: https://www.geotis.de/homepage/references, August 07, 2024.

[22] A.M. Przybycin, M. Scheck-Wenderoth, M. Schneider, The origin of deep geothermal anomalies in the German molasse basin: results from 3D numerical models of coupled fluid flow and heat transport, Geotherm. Energy 5 (1) (2017), https://doi.org/10.1186/s40517-016-0059-3.

[23] Esri. Arcgis Pro (Version 3.2.1). Esri Inc.

[24] C. Arpagaus, F. Bless, M. Uhlmann, J. Schiffmann, S. Bertsch, High temperature heat pumps: market overview, state of the art, research status, refrigerants, and application potentials, Energy (2018) 1–10, https://doi.org/10.1016/j.energy.2018.03.166.

[25] C. Arpagaus, L. Brendel, S. Paranjape, F. Bless, M. Uhlmann, S. Bertsch, New Developments and Products for Supply Temperatures Above 100 °C, 2023.

[26] J. Jiang, B. Hu, R.Z. Wang, N. Deng, F. Cao, C.-C. Wang, A review and perspective on industry high-temperature heat pumps, Renew. Sustain. Energy Rev. 161 (2022) 112106, https://doi.org/10.1016/j.rser.2022.112106.

[27] K.-M. Adamson, T.G. Walmsley, J.K. Carson, Q. Chen, F. Schlosser, L. Kong, et al., High-temperature and transcritical heat pump cycles and advancements: a review, Renew. Sustain. Energy Rev. 167 (2022) 112798, https://doi.org/10.1016/j.rser.2022.112798.

[28] H. Khalid, S. Uzair, M.U. Ahrens, S. Ren, P. Ganesan, I. Tolstorebrov, et al., Potential evaluation of integrated high temperature heat pumps: a review of recent advances, Appl. Therm. Eng. 230 (2023) 120720, https://doi.org/10.1016/j.applthermaleng.2023.120720.

[29] J. Barco-Burgos, J.C. Bruno, U. Eicker, A.L. Saldaña-Robles, V. Alcántar-Camarena, Review on the integration of high-temperature heat pumps in district heating and cooling networks, Energy 239 (2022) 122378, https://doi.org/10.1016/j.energy.2021.122378.

[30] G. Kosmadakis, C. Arpagaus, P. Neofytou, S. Bertsch, Techno-economic analysis of high-temperature heat pumps with low-global warming potential refrigerants for upgrading waste heat up to 150 °C, Energy Convers. Manag. 226 (2020) 113488, https://doi.org/10.1016/j.enconman.2020.113488.

[31] M. Dumont, R. Wang, D. Wenzke, K. Blok, R. Heijungs, The techno-economic integrability of high-temperature heat pumps for decarbonizing process heat in the food and beverages industry, Resour. Conserv. Recycl. 188 (2023) 106605, https://doi.org/10.1016/j.resconrec.2022.106605.

[32] C. Mateu-Royo, S. Sawalha, A. Mota-Babiloni, J. Navarro-Esbrí, High temperature heat pump integration into district heating network, Energy Convers. Manag. 210 (2020) 112719, https://doi.org/10.1016/j.enconman.2020.112719.

[33] O. Arslan, A.E. Arslan, I. Kurtbas, Exergoeconomic and exergoenvironmental based multi-criteria optimization of a new geothermal district heating system integrated with thermal energy storage driven heat pump, J. Build. Eng. 73 (2023) 106733, https://doi.org/10.1016/j.jobe.2023.106733.

[34] D.-X. Liu, H.-Y. Lei, J.-S. Li, C.-S. Dai, R. Xue, X. Liu, Optimization of a district heating system coupled with a deep open-loop geothermal well and heat pumps, Renew. Energy 223 (2024) 119991, https://doi.org/10.1016/j.renene.2024.119991.

[35] K. Sartor, V. Lemort, P. Dewallef, Improved district heating network operation by the integration of high-temperature heat pumps, Int. J. Sustain. Energy 37 (9) (2018) 842–856, https://doi.org/10.1080/14786451.2017.1383409.

[36] S. Dimitriu, A.-M. Bianchi, F. Baltaretu, The up-to-date heat pump-combined heat and power solution for the complete utilization of the low enthalpy geothermal water potential, Intern. J. Energy Environ. Eng. 8 (3) (2017) 189–196, https://doi.org/10.1007/s40095-014-0145-x.

[37] J.K. Jensen, T. Ommen, W.B. Markussen, B. Elmegaard, Design of serially connected district heating heat pumps utilising a geothermal heat source, Energy 137 (2017) 865–877, https://doi.org/10.1016/j.energy.2017.03.164.

[38] J. Jeßberger, F. Heberle, D. Brüggemann, Maximising the potential of deep geothermal energy: thermal output increase by large-scale heat pumps, Appl. Therm. Eng. 257 (2024) 124240, https://doi.org/10.1016/j.applthermaleng.2024.124240.

[39] J. Deng, Y. Su, C. Peng, W. Qiang, W. Cai, Q. Wei, et al., How to improve the energy performance of mid-deep geothermal heat pump systems: optimization of heat pump, system configuration and control strategy, Energy 285 (2023), https://doi.org/10.1016/j.energy.2023.129537.

[40] H. Arat, O. Arslan, Exergoeconomic analysis of district heating system boosted by the geothermal heat pump, Energy 119 (2017) 1159–1170, https://doi.org/10.1016/j.energy.2016.11.073.

[41] A.R. Mazhar, S. Liu, A. Shukla, A state of art review on the district heating systems, Renew. Sustain. Energy Rev. 96 (2018) 420–439, https://doi.org/10.1016/j.rser.2018.08.005.

[42] J. Jeßberger, F. Heberle, D. Brüggemann, Integration of high-temperature heat pumps into geothermal energy systems, in: 10th HEAT POWERED CYCLES Conference, 2023, pp. 16–30.

[43] L.F. Moody, Friction factors for pipe flow, J. Fluid Eng. 66 (8) (1944) 671–678, https://doi.org/10.1115/1.4018140.

[44] P. Schlagermann, Exergoökonomische Analyse Geothermischer Strombereitstellung am Beispiel Des Oberrheingrabens [Dissertation], Technische Universität München, München, 2014.
[45] J. Jeßberger, C. Arpagaus, F. Heberle, L. Brendel, S. Bertsch, D. Brüggemann, Experimental investigations of upscaling effects of high-temperature heat pumps with R1233zd(E), Int. J. Refrig. 164 (2024) 243–256, https://doi.org/10.1016/j.ijrefrig.2024.04.023.
[46] C. Arpagaus, F. Bless, M. Uhlmann, J. Schiffmann, S. Bertsch, High temperature heat pumps: market overview, state of the art, research status, refrigerants, and application potentials, Intern. Refriger. Air Condition. Confere. (2018) 1–10.
[47] J. Jiang, B. Hu, R.Z. Wang, N. Deng, F. Cao, C.-C. Wang, A review and perspective on industry high-temperature heat pumps, Renew. Sustain. Energy Rev. 161 (2022) 112106, https://doi.org/10.1016/j.rser.2022.112106.
[48] Agora Energiewende, I.E.G. Fraunhofer, Roll-out Von Großwärmepumpen in Deutschland: Strategien Für Den Markthochlauf in Wärmenetzen Und Industrie, 01th ed, 2023.
[49] Verein Deutscher Ingenieure, Wirtschaftlichkeit Gebäudetechnischer Anlagen (2067), Beuth Verlag GmbH, Berlin, 2012.
[50] Statista, Inflationsrate in Deutschland von 1992 bis 2023. https://de.statista.com/statistik/daten/studie/1046/umfrage/inflationsrate-veraenderung-des-verbraucherpreisindexes-zum-vorjahr/, December 09, 2024.
[51] European Central Bank, Key ECB interest rates. https://www.ecb.europa.eu/stats/policy_and_exchange_rates/key_ecb_interest_rates/html/index.en.html, December 09, 2024.
[52] Erdwerk GmbH, Drilling Costs medium-deep Geothermal Systems. Call, 2023.
[53] C. Arpagaus, L. Brendel, S. Paranjape, F. Bless, M. Uhlmann, S. Bertsch, New Developments and Products for Supply Temperatures Above 100 °C, 2023.
[54] Geothermal heating plant operator. Service life of the ESP, Call (2022).
[55] Statistisches Bundesamt, Daten zur Energiepreisentwicklung DESTATIS. https://www.destatis.de/DE/Themen/Wirtschaft/Preise/Publikationen/Energiepreise/energiepreisentwicklung-pdf-5619001.html, February 05, 2024.
[56] Verein Deutscher Ingenieure, Betriebswirtschaftliche Berechnungen Für Investitionsgüter Und Anlagen;Ics 03.100.01, 91.140.10(VDI 6025), Beuth Verlag GmbH, Berlin, 2012.
[57] AGFW | Der Energieeffizienzverband für Wärme, Kälte und KWK e. V. Preis* für Fernwärme nach Anschlusswert in Deutschland in den Jahren 1991 bis 2023 (in Euro pro Megawattstunde) Statista. https://de.statista.com/statistik/daten/studie/250114/umfrage/preis-fuer-fernwaerme-nach-anschlusswert-in-deutschland/, August 14, 2024.
[58] Bundesamt Für Wirtschaft Und Ausfuhrkontrolle, BEW-Merkblatt Antragstellung, 2022.
[59] C. Arpagaus, L. Brendel, S. Paranjape, F. Bless, M. Uhlmann, S. Bertsch, New developments and products for supply temperatures above 100 °C. https://022fdef7-26ea-4db0-a396-ec438d3c7851.filesusr.com/ugd/c1ceb4_4c566f4ba92f4db4a7ee45a2ec951ff3.pdf, October 28, 2024.
[60] European Environment Agency, Greenhouse gas emissions from energy use in buildings in Europe. https://www.eea.europa.eu/en/analysis/indicators/greenhouse-gas-emissions-from-energy?activeAccordion=ecdb3bcf-bbe9-4978-b5cf-0b136399d9f8, 2023, 24.09.24.
[61] Umweltbundesamt. Energieverbrauch für fossile und erneuerbare Wärme; Available from: https://www.umweltbundesamt.de/daten/energie/energieverbrauch-fuer-fossile-erneuerbare-waerme.
[62] T. Lauf, Memmler, Michael, S. Schneider, Emissionsbilanz erneuerbarer Energieträger: bestimmung der vermiedenen Emissionen im Jahr, Clim. Change (2022). Dessau-Roßlau, https://www.umweltbundesamt.de/sites/default/files/medien/11850/publikationen/20231219_49_2023_cc_emissionsbilanz_erneuerbarer_energien_2022_bf.pdf. (Accessed 15 August 2024).
[63] EU Technical Expert Group on Sustainable Finance. Taxonomy report: Technical Annex; Available from: https://finance.ec.europa.eu/system/files/2020-03/200309-sustainable-finance-teg-final-report-taxonomy-annexes_en.pdf. [March 5, 2023].
[64] C. Lohse, Environmental impact by hydrogeothermal energy generation in low-enthalpy regions, Renew. Energy 128 (2018) 509–519, https://doi.org/10.1016/j.renene.2017.06.030.
[65] K. Menberg, F. Heberle, H. Uhrmann, C. Bott, S. Grünäugl, D. Brüggemann, et al., Environmental impact of cogeneration in binary geothermal plants, Renew. Energy 218 (2023) 119251, https://doi.org/10.1016/j.renene.2023.119251.
[66] M.R. Karlsdóttir, Pálsson Óp, H. Pálsson, L. Maya-Drysdale, Life cycle inventory of a flash geothermal combined heat and power plant located in Iceland, Int. J. Life Cycle Assess. 20 (4) (2015) 503–519, https://doi.org/10.1007/s11367-014-0842-y.
[67] A. Pratiwi, G. Ravier, A. Genter, Life-cycle climate-change impact assessment of enhanced geothermal system plants in the upper rhine valley, Geothermics 75 (2018) 26–39, https://doi.org/10.1016/j.geothermics.2018.03.012.
[68] J. Sadhukhan, Net zero electricity systems in global economies by life cycle assessment (LCA) considering ecosystem, health, monetization, and soil CO2 sequestration impacts, Renew. Energy 184 (2022) 960–974, https://doi.org/10.1016/j.renene.2021.12.024.
[69] M. Douziech, L. Tosti, N. Ferrara, M.L. Parisi, P. Pérez-López, G. Ravier, Applying harmonised geothermal life cycle assessment guidelines to the rittershoffen geothermal heat plant, Energies 14 (13) (2021) 3820, https://doi.org/10.3390/en14133820.
[70] R. Zhang, G. Wang, X. Shen, J. Wang, X. Tan, S. Feng, et al., Is geothermal heating environmentally superior than coal fired heating in China? Renew. Sustain. Energy Rev. 131 (2020) 110014 https://doi.org/10.1016/j.rser.2020.110014.
[71] A.S. Pratiwi, E. Trutnevyte, Life cycle assessment of shallow to medium-depth geothermal heating and cooling networks in the state of Geneva, Geothermics 90 (2021) 101988, https://doi.org/10.1016/j.geothermics.2020.101988.
[72] International Organization for Standardization, Environmental Management - Life Cycle Assessment -Requirements and guidelines;13.020.10(14044:2006), Beuth Verlag GmbH, Berlin, D, 2006.
[73] International Organization for Standardization, Environmental Management - Life Cycle Assessment - Principles and Framework, first ed., Brüssel: Beuth, 2020, 13.020.10; 13.020.60(14040:2006).
[74] M.L. Parisi, M. Douziech, L. Tosti, P. Pérez-López, B. Mendecka, S. Ulgiati, et al., Definition of LCA guidelines in the geothermal sector to enhance result comparability, Energies 13 (13) (2020) 1–18, https://doi.org/10.3390/en13143534, 3534.
[75] S. Frick, M. Kaltschmitt, G. Schröder, Life cycle assessment of geothermal binary power plants using enhanced low-temperature reservoirs, Energy 35 (5) (2010) 2281–2294, https://doi.org/10.1016/j.energy.2010.02.016.
[76] A.S. Pratiwi, E. Trutnevyte, Life cycle assessment of shallow to medium-depth geothermal heating and cooling networks in the state of Geneva, Geothermics 90 (Suppl) (2021) 101988, https://doi.org/10.1016/j.geothermics.2020.101988.
[77] S. Fattler, J. Conrad, A. Regett, F. Böing, A. Guminski, S. Greif, et al., Dynamis - Hauptbericht: Dynamische und intersektorale Maßnahmenbewertung zur kosteneffizienten Dekarbonisierung des Energiesystems. https://www.ffe.de/projekte/dynamis/. (Accessed 15 December 2023).
[78] PRé sustainability. SimaPro, Available from: https://simapro.com/. (Accessed 25 October 2024).
[79] S. Andreasi Bassi, F. Biganzoli, N. Ferrara, A. Amadei, A. Valente, S. Sala, et al., Updated Characterisation and Normalisation Factors for the Environmental Footprint 3.1 Method, Publications Office of the European Union, Luxembourg, 2023.
[80] A.C. Violante, F. Donato, G. Guidi, M. Proposito, Comparative life cycle assessment of the ground source heat pump vs air source heat pump, Renew. Energy 188 (2022) 1029–1037, https://doi.org/10.1016/j.renene.2022.02.075.
[81] Umweltbundesamt, Tabellarische Aufstellung Der Abgeleiteten Emissionsfaktoren Für CO2, Energie & Industrieprozesse, 2024. Available from: https://www.umweltbundesamt.de/daten/klima/treibhausgas-emissionen-in-deutschland#nationale-und-europaische-klimaziele. (Accessed 17 September 2024).
[82] A.T. McCay, M.E.J. Feliks, J.J. Roberts, Life cycle assessment of the carbon intensity of deep geothermal heat systems: a case study from Scotland, Sci. Total Environ. 685 (2019) 208–219, https://doi.org/10.1016/j.scitotenv.2019.05.311.
[83] S.-Y. Pan, M. Gao, K.J. Shah, J. Zheng, S.-L. Pei, P.-C. Chiang, Establishment of enhanced geothermal energy utilization plans: barriers and strategies, Renew. Energy 132 (2019) 19–32, https://doi.org/10.1016/j.renene.2018.07.126.
[84] F. Schölderle, G. Götzl, F. Einsiedl, K. Zosseder, Uncertainty assessment of corrected bottom-hole temperatures based on monte carlo techniques, Energies 15 (17) (2022) 6367. https://doi.org/10.3390/en15176367.